Analysis of jet-noise-reduction concepts by large-eddy simulation

by

Michael L. Shur, Philippe R. Spalart**,
Michael Kh. Strelets and Andrey V. Garbaruk

reprinted from

international journal of aeroacoustics

volume 6 · number 3 · 2007

published by MULTI-SCIENCE PUBLISHING CO. LTD.,
5 Wates Way, Brentwood, Essex, CM15 9TB UK
E-MAIL: mscience@globalnet.co.uk
WEBSITE: www.multi-science.co.uk

Analysis of jet-noise-reduction concepts by large-eddy simulation

Michael L. Shur*, Philippe R. Spalart, Michael Kh. Strelets***, and Andrey V. Garbaruk#**

**New Technologies and Services (NTS), St.-Petersburg 197198, Russia; mshur@rscac.spb.ru*
***Boeing Commercial Airplanes, P.O. Box 3707 Seattle, WA 98124, USA, philippe.r.spalart@boeing.com*
****New Technologies and Services (NTS), St.-Petersburg 197198, Russia; strelets@mail.rcom.ru*
 # St.-Petersburg State Polytechnic University, St.-Petersburg 195220, Russia; agarbaruk@rscac.spb.ru

ABSTRACT

The paper outlines the latest improvements to a CFD/CAA numerical system developed by the authors starting in 2001, and presents its application to the evaluation of three noise-reduction concepts. The improvements include a two-step RANS-LES approach to represent complex nozzles much more faithfully, and an accurate algorithm for shock capturing in LES, now based on local automatic activation of flux-limiters. The noise-reduction concepts considered are: beveled nozzles, dual nozzles with fan-flow deflection, and chevron nozzles. The simulations are carried out on PC clusters with at most six processors and on rather modest grids (2-4 million nodes). Nonetheless, in most cases the system is close to the 2-3 dB target accuracy both in terms of directivity and spectrum, while limited in terms of frequency (to a diameter Strouhal number that ranges from 2 to 4, depending on the grid used and the flow regime). Although this limitation is significant, especially for chevron nozzles, the overall message of the paper is that the available CFD/CAA numerical and physical models, properly combined, are capable of predicting the noise of rather complex jets with affordable computational resources, and already today can be helpful in the rapid low-cost analysis of noise-reduction concepts.

1. INTRODUCTION

In engineering practice, the prediction of noise from jet engines is still based on empirical methods and scaling laws such as Lighthill's or, at most, on steady Reynolds-Averaged-Navier-Stokes (RANS) computations combined with *ad hoc* models for noise sources. The empirical basis of the latter methods and extreme simplifications of the turbulence responsible for noise generation appear to rule them out as trustworthy tools for the evaluation of new concepts of noise reduction. Such a tool must deal with many non-trivial features, like wide temperature differences, two-stream flows, imperfectly expanded sonic and supersonic streams, jets in an ambient flow (in flight), non-circular nozzles, *etc*., and must be capable of accounting for the subtle effects of design innovations on the turbulent structures responsible for the noise.

These considerations, increasing computing power, and advancing algorithms are the factors driving the field towards Large Eddy Simulation (LES), the only turbulence-resolving approach feasible at high Reynolds numbers. The application of LES to jet-noise prediction is under way in many research groups now (see the references in Refs. 1, 2 and the latest publications (Refs. 3-12)). However most of the studies are more "academic" than "industrial" in that they deal with simple round jets (many of the codes lacking general-geometry capabilities) and very few of the "complicating factors" mentioned above. This is partly explained by the extreme demands on the numerical system in order to resolve multiple turbulent scales and by the complexity of combining turbulence and far-field acoustics. Boosting the usefulness of the method therefore means eliminating any waste of computing effort. This highlights the importance of a number of decisions needed for LES-based noise computation, both in the turbulence-simulation and the sound-extraction approaches. LES brings up options for: the configuration of the computational domain and topology of the grid; the numerical scheme and boundary conditions; the Subgrid-Scale (SGS) model (if any); the approach to obtaining transition to turbulence, *etc*. For noise extraction, decisions are needed on using direct or integral methods and, for the latter, on a Kirchhoff or Ffowcs-Williams/Hawkings (FWH) formulation, the shape and position of control surfaces, their treatment near the downstream end, *etc*. All these decisions should be assessed not only separately but as an aggregate as well. An analysis of the state of the art (Ref. 1) shows that the range of approaches being explored remains wide, and that the CFD/CAA community is still far from a consensus on the most efficient one. This is fairly normal, considering the complexity of the problem.

In this paper, we present results illustrating the capabilities of the non-empirical LES/FWH-based numerical system (Ref. 1) as a tool for evaluation of noise-reductions concepts. The system has been developed by the authors over the last 5 years with the final goal of predicting the noise of realistic engine jets within 2-3 dB accuracy over as wide frequency range as possible. The approach seems to combine sensibly some elements of the techniques used in the literature with some new ones and, based on the results presented in Refs. 1, 2 and in this paper, is rather promising. This is the case although the levels of accuracy and geometry completeness reached are, of course, still not sufficient for airliner certification, and will not be for many years, especially as far as the high-frequency noise is concerned (semi-theoretical work is underway to extend the LES spectrum to higher frequencies). However, the extrapolation from laboratory experiments to certification also has its many uncertainties, and flow measurements capable of "explaining" the success or failure of a device are close to impossible, whereas LES provides the entire flow and sound fields. Therefore, the present value of the method also lies precisely in helping a more educated, rapid, and low-cost evaluation of noise-reduction devices. LES also sets no limits to the ambient flow velocity, in contrast with most experimental facilities. The enhanced understanding of flow physics will also, sooner or later, lead to an invention.

The paper is organized as follows. In Section 2 a brief presentation is given of the numerical system outlined in more detail in Ref. 1, and then its latest developments are presented. Then, in Sections 3-5, results are discussed of the evaluation of three noise reduction concepts, namely, two relatively recent ones suggested by Viswanathan [13], [14] (beveled nozzles) and Papamoschou [15] (fan-flow deflecting vanes), and then the well-known chevron nozzle concept. Finally, the conclusion section summarizes major achievements and outlines still-unresolved problems.

2. OVERVIEW OF THE NUMERICAL SYSTEM

A detailed description of the numerical approach used in the present work is given in Refs. 1, 2, and a self-contained description of it would take too much space here. In this Section we briefly outline the salient features of this system and present the latest improvements, aimed at a more realistic prediction of the complex jets typical of innovative low-noise designs for aircraft engine installations.

2.1. Numerical approach of refs. 1, 2

The approach is implemented in the NTS code [16], which runs on structured multi-block curvilinear grids with implicit 2nd order time integration and dual time stepping. The inviscid differencing is based on the flux-difference splitting scheme of Roe [17]. It is a weighted average of 4th-order centered and 5th-order upwind-biased schemes (with typical weights 0.75 and 0.25, respectively) in the turbulent region and acoustic near field, and "pure" upwind-biased outside that region. Using these weights, the numerical dissipation is kept at the lowest level that will prevent numerical instabilities introduced by nonlinearities, grid stretching, and other sources.

For the turbulence simulation, the current choice is to de-activate the Subgrid-Scale (SGS) model and to rely on the subtle numerical dissipation of the slightly upwind scheme, a strategy which is compatible with the spirit of LES, away from walls. This choice is dictated mostly by the crucial importance of a realistic representation of the transition to turbulence in the jet shear layers, which should be provided by the CFD approach for purposes of noise prediction. This representation is inevitably approximate, since resolving the fine-scale turbulent structures of the nozzle boundary layers that seed the shear layer and influence its rapid transition in the real high-Re jets is far out of reach. Other LES strategies that were tested turned out visibly less successful. For instance, if the SGS model is activated, the transition to turbulence is crucially delayed. If only the upwind-biased (3rd or 5th order) schemes are used, the delay also is very pronounced, due to more dissipative numerics. Frequent filtering, as used in some codes along with centered differencing, may well have the same effect. Artificial inflow forcing, as employed in many other jet studies, could resolve this issue to some extent, but was rejected to avoid the creation of parasitic noise and especially the introduction of a number of arbitrary parameters. The issue of whether forcing is justified is likely to remain controversial until natural forcing by LES eddies in the nozzle flow is affordable, and for a thin enough boundary layer. Our results without forcing certainly benefit from having thin boundary layers, which reduces the extent of the unrealistic transition region, and the azimuthal correlation scale.

For noise prediction, the far-field formulation of the permeable Ffowcs-Williams/Hawkings surface integral method (see Refs. 18,19) is used without external quadrupoles, which seems to be the best compromise between efficiency and accuracy. In contrast to the Kirchhoff approach, which could be the other practical option, it allows the placement of the majority of the control surface in the immediate vicinity of the turbulent region (in the inviscid but non-linear near-field) and, therefore, the confinement of the fine-grid area needed for turbulence resolution exactly to this turbulent area (Ref. 20). Although the coarsening of the grid towards the outer boundaries does need to be very gradual to avoid spurious noise generation, the rest of the grid is essentially a “cushion” which absorbs outgoing waves better than a tightly-fitted numerical boundary condition would.

The best shapes for the FWH surfaces around a jet are tapered funnels; this minimizes the loss of quality of the waves before they reach the surface, particularly for the higher-frequency waves near the nozzle. The funnel then has a “closing disk” of some sort, which turbulence necessarily crosses, in violation of the assumptions of the quadrupole-less FWH approach. Possible options in this thorny issue include simply omitting the disk from the integral, and including it as if all the assumptions were satisfied; neither one is accurate enough in general, particularly for hot jets, and a change of variables was implemented. It was shown in Ref. 1 that, with a thorough treatment of the FWH formula and an optimal choice of variables, closing the FWH surfaces at the outflow end results in a better prediction of both noise spectra and overall sound intensity. A more compelling interpretation of the change of variable with a clearer equation has been derived, and will be published separately along with new tests. The equation is contained in Ref. 36, and it was also found that the variable is one used by Goldstein [37] since 2001. Besides, the arguments made in favor of open surfaces have been found to be mathematically weak; in particular the stationary-phase method applies only to line integrals, and not to surface integrals (Ref. 21).

A typical grid and FWH surface are shown in Fig. 1. Along with the jet plume area, the computational domain contains the outer region around the nozzle wall, which is necessary for a correct prediction of sound propagating upstream. The full LES domain is much larger than the FWH domain. For jets in still air, the FWH domain typically extends to 25-30 jet diameters, D_{jet}, streamwise, and the full domain including the buffer layer is 50-60 D_{jet}. This provides damping of the fluctuations in this area and weakens wave reflections at the boundaries. In the simulations of jets in flight, due to the protracted decay of the turbulence, the computational domain is extended in the streamwise direction up to about 80 D_{jet}, with the FWH surfaces as long as 50 D_{jet}. The grid has two overlapping blocks (additional artificial blocks are introduced to better make use of parallel processors). This topology seems close to optimal for 3D computations of round and near-round jets. The inner, Cartesian, block is helpful in avoiding a singularity at the axis of the cylindrical coordinates and the outer, O-type, block allows a good control of the grid density and, in particular, a fine distribution where the thin shear layer is located. This issue is cited as very important by Bodony and Lele [22]. The streamwise and azimuthal grid spacings are not as fine as the radial spacing, of course; the grid is not isotropic, and neither are the dominant eddies of a transitioning mixing layer. Only these eddies can be captured in this region, and this region does not have Kolmogorov turbulence, which would motivate isotropic cells.

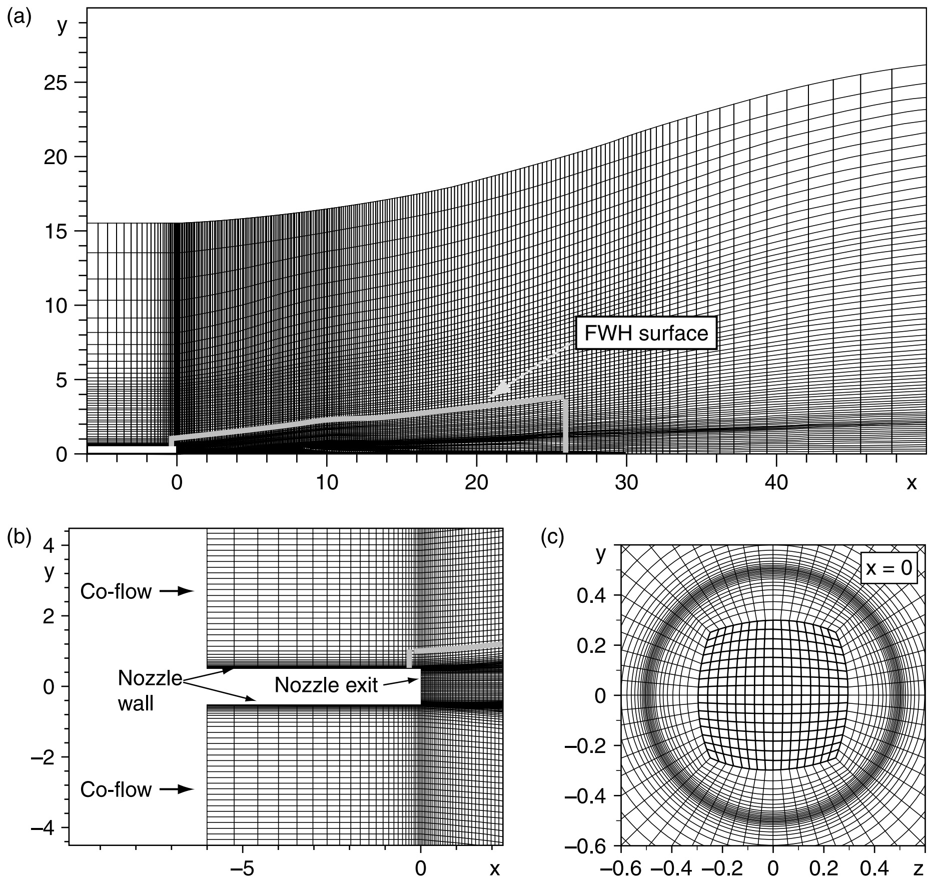

Figure 1: Typical grid and FWH surface: side view through axis (a), vicinity of the nozzle exit (b), and end view at nozzle exit (c). Lengths normalized with jet diameter.

Fully Cartesian or fully cylindrical topologies seem much less efficient; implicit time integration is also essential in this matter. Note that the computational domain shown in Fig. 1 does not include the interior of the nozzle. This was the way the simulations in Refs. 1,2 were performed: the jet conditions were prescribed as inflow boundary conditions at the nozzle exit.

The numerical system briefly presented above has been applied to a wide range of round jets. These studies showed that it provides a realistic description of the shear-layer roll-up and three-dimensionalization, even in jets in ambient flow with velocity up to 60% of the jet's. This turns out possible thanks to a global instability sustained by the jet-flow when a velocity profile with a thin enough boundary layer is prescribed at the nozzle exit, and with the high-order numerics used. Other effects that have been predicted with good reliability include: Mach-number variation for isothermal jets; cross-effect between the acoustic Mach number and jet heating; effect of flight on both isothermal and hot jets; effect of shock-cell/turbulence interaction in a sonic slightly under-expanded jet (fully expanded Mach number $M_{FE} = 1.37$). These simulations, although performed with relatively small grid counts (on the order of one million nodes) resulted in fairly good agreement with experimental data on mean flow and turbulence statistics (when available) and in noise predictions close to the target accuracy of 2-3 dB both in overall directivity and spectra up to the diameter-based Strouhal number $St \approx 1.5$.

In general, the findings of Refs. 1, 2 are encouraging, support the credibility of the approach, and justify its application to more complex flows, thus progressing in the direction of airliner engines. However, as already mentioned, none of the simulations presented in Refs. 1, 2 include the interior of the nozzle. Instead, the jet flow conditions are prescribed analytically as inflow boundary conditions at the nozzle exit, which assumes that the jet has a simple behavior in the core, and a thin near-wall boundary layer that may be specified somewhat arbitrarily (experimental studies essentially never report the boundary-layer thickness). For simple jets from single round nozzles this approach is quite justified, but beyond this "academic", area, i.e., for jets from complex (e.g., beveled or dual, staggered and offset) nozzles it is insufficient, since a strong non-uniformity of the static pressure in the nozzle exit plane and a vectoring of the jet plume are typical of such cases, and therefore, no a-priori boundary conditions at the exit of such nozzles can be formulated that are sufficiently accurate.

Another focus for improvement is that, for cases with shocks (under-expanded sonic and supersonic jets), the algorithm used in Refs. 1, 2 (introducing zonal flux limiters) causes too smooth a transition to turbulence, due to increased dissipation in the numerics. A consequence is some contamination of the sound spectra.

Below we present the latest improvements of the numerical system of Refs. 1, 2 which are aimed at resolving these two important issues.

2.2. Latest improvements of the numerical system

2.2.1 Two-step, RANS-LES, approach

The only fully thorough way of treating jets from complex nozzles is full-scale coupled nozzle-plume LES. Unfortunately, at practical Reynolds numbers, this is currently unaffordable because the viscous sublayer of the turbulent boundary layer is too thin. In order to resolve this issue, Andersson et al. [3,4] arbitrarily reduce the Reynolds number in their nozzle-plume LES down to an affordable value, while the ONERA team (Refs. 12, 23) perform Implicit LES (deactivating the SGS model) not only in the jet-plume, but inside the nozzle as well. Both approaches result in a significant and non-controlled thickening of the nozzle boundary layers, which, in turn, may affect the transition to turbulence in the jet shear layer and, as a result, in a deterioration of the high-frequency part of the noise-spectrum.

An alternate way to capture the effect of the internal nozzle geometry and maintain realistic boundary layers without the extreme cost of a coupled nozzle-plume LES is to apply a two-stage RANS-LES simulation strategy as developed and tested in Refs. 24, 25 and in the present work.

In the first stage, a coupled nozzle-plume RANS computation is performed, axisymmetric or 3D depending on the geometry. If 3D, this is not trivial, but still is quite affordable with grids fine enough to resolve all the nozzles' boundary layers; in any case, it is incomparably less expensive than a full LES.

In the second stage, LES is carried out for the jet plume only with inflow conditions at the nozzle exit taken from the RANS solution obtained in the first step. Note that the minimum grid spacing in the radial direction at the nozzle wall edge used in this LES stage may be 20 times coarser than in the RANS grid, resolving the viscous sublayer not being necessary. This saves around 15 points per boundary layer and, what is much more important, permits a crucial (order of magnitude) increase of the time step of the integration. This is precisely what makes LES possible, without loss of realism, since the viscous sublayer rapidly disintegrates into the free shear layer. The turbulence effects in the RANS are not as accurate as in the LES, naturally, but their upstream influence to the nozzle exit and into the nozzle is weak. The dominant effects targeted by this two-step approach are inviscid. The RANS uses the $v_t - 92$ model of Ref. 26 (see also Ref. 27). This is a one-equation, eddy viscosity transport model similar to the Spalart-Allmaras model (Ref. 28) but having special terms tuned to predict the axisymmetric flows and to account for the compressibility effects, which is important for jets.

The specific form of the inflow conditions used depends on whether the inflow is subsonic or supersonic.

For subsonic inflow, we impose (after interpolation of the RANS solution to the LES grid) the profiles of stagnation pressure and temperature, p_t and T_t, and of the inflow "velocity angles" α_y and α_z defined as:

$$\tan(\alpha_y) = u_y / u_x,\ \tan(\alpha_z) = u_z / u_x, \tag{1}$$

where u_x, u_y and u_z are the Cartesian components of the velocity vector. In most cases to date, the stagnation pressure and temperature have been uniform outside the boundary layers, and the angles in eqn (1) have been the crucial product of the RANS solution.

As for the static pressure, just as in all the previous simulations (Refs. 1, 2), the 1D non-reflecting boundary condition of Engquist and Majda [29] is used:

$$\partial p / \partial t - \max\{(c - u_l), 0\} \cdot (\partial p / \partial l) = 0\ , \tag{2}$$

where $(\partial/\partial l)$ denotes differentiation along the streamwise grid line, u_l is the corresponding velocity component, and c is the local speed of sound.

For supersonic inflow, all the flow parameters are simply specified from the RANS solution.

Sections 3 and 5 will show that the approach outlined above turns out to be not only feasible, but capable of predicting the noise of jets from rather complex nozzles with a reasonably high accuracy.

2.2.2. Local automatic flux-limiters for jets with shocks

Shock cells, which are often present in airplanes' exhaust jets in cruise flight, are of great importance in the airliner industry. The shocks, naturally, raise the level of numerical difficulty. The demands of shock capturing and those of LES resolution with acceptable numerical dissipation conflict. Probably for this reason, no examples of LES of jets with shock-cells using high-order numerical schemes are found in the literature. The approach to shock capturing in LES developed and tested in Refs. 1, 2 turned out to be rather efficient, and permitted to reconcile to some extent these contradictory demands. Recall that this approach employs a *zonal* activation (in an a-priori area prescribed analytically where strong shocks are expected) of the Van Albada flux-limiter (Ref. 30) and switching from the 5th to 3rd order scheme in the upwind component of the hybrid (centered/upwind-biased) numerics used in the NTS code everywhere else. This effectively suppressed the instability of the hybrid low-dissipation scheme, caused by the interaction of shocks with turbulence for the sonic slightly under-expanded jet of Tanna [31] considered in Ref. 2. At the same time, based on "numerical Schlierens" and density fields from the simulation, it was found that there were no spurious oscillations, the shocks were not smeared, and the physical instability of neither the shocks nor the shear layer was suppressed. However, the zone with active limiters could not include the shear layers (otherwise the transition to turbulence was suppressed) and so, in order to preserve numerical stability, the weight of the upwind differences in the hybrid scheme had to be raised in the initial region of the shear layers (see Ref. 1). This led to insufficient accuracy in the representation of transition to turbulence and, as a result, to the appearance of false peaks in the noise spectra (Ref. 2). This and, also, the obvious difficulty of applying a zonal method to complex jets with an a-priori unclear shock topology, was the motivation to search for another technique, more robust and flexible, as presented now.

Unlike the zonal method of Refs. 1, 2 the new one is based on an algorithm with local *automatic* activation of the flux-limiters, in the spirit of the work of Hill and Pullin [32]. The limiters are introduced independently in different spatial directions. As an example, let us consider the direction i in the computational coordinates.

When computing the inviscid fluxes at the cell face $(i+1/2)$, the standard NTS' hybrid numerics are replaced with the pure upwind-biased 3rd order differencing, and the van Albada flux-limiters are activated, if the inequality

$$\frac{|p_{i+1}-p_i|}{\min\{p_i, p_{i+1}\}} > \varepsilon \tag{3}$$

is satisfied. Here, p is the pressure, and the parameter ε is set equal 0.5, based on preliminary numerical experiments.

In accordance with this inequality, the standard numerics are locally replaced by the more dissipative scheme with flux-limiters in the event that the pressure change between the two adjacent control volumes is "too large". Provided that the grid used ensures an adequate resolution of "smooth" flow regions, this occurs only at strong enough shocks. Knowing that shocks in turbulent jets are not stationary (but fluctuate), switching to 3rd order upwinding and turning on the flux-limiters is carried out not only at the cell face $(i+1/2)$, where the inequality (3) is satisfied, but also at two neighboring faces, $(i-1/2)$ and $(i+3/2)$. Other than that, in order to accelerate the sub-iteration convergence, the flux-limiters are "frozen" after 2 sub-iterations within a time-step.

The algorithm described above has been tested on the cold and hot round jets studied in the experiments of Tanna [31] and Vishwanathan [13] and was shown to be much more accurate than the zonal one used in Ref. 2 (see Ref. 33 for more detail). In this work it is applied to the beveled nozzles within the coupled RANS/LES approach.

3. JETS FROM BEVELED NOZZLES

The motivation to this study is multi-fold. First of all, according to the experiments of Viswanathan [13, 14], who has proposed this innovation, beveled nozzles cause a noticeable jet noise reduction. Also, regardless of the industrial value of the concept, the unique jet-noise study accumulated in the experiments [13, 14] presents in itself a very attractive database for validation of CFD/CAA approaches. Additionally, CFD/CAA may be helpful in supporting the experiments, in terms of elucidating physical mechanisms responsible for the noise reduction, and probably even an optimisation of the designs.

In terms of CFD, the exercise is challenging, first of all, because due to the strong non-uniformity of the static pressure in the nozzle exit plane and the plume vectoring, even single beveled nozzle flows should be computed with the use of the two-stage RANS-LES technology. In this section this technology is applied to hot ($T_t / T_a = 3.2$) jets from baseline round and beveled nozzles with bevel angle of 45° (see Fig. 2) at 3 different values of the nozzle pressure ratio, NPR [13]: $NPR = 1.28$ (fully-expanded jet Mach number M_{FE}=0.6), $NPR = 1.89$ (M_{FE}=1 − sonic perfectly expanded jet), and $NPR = 4.0$ (M_{FE}=1.56 – sonic strongly under-expanded jet).

A fragment of the grid used in the LES stage of the computations, together with a vorticity snapshot from the beveled jet and the nested FWH surfaces are shown in Fig. 3. Note how both the grid and the FWH surfaces are adjusted to the plume vectoring. This preserves accuracy without inflating the total number of nodes in the simulations, which varied from around 1.5 million nodes for the subsonic jets up to 3.6 million nodes for the under-expanded jets.

Figure 4 illustrates the effects of nozzle beveling and Mach number on the general flow pattern and turbulence structure. In particular, the figure displays a non-linear growth of the beveled plume deflection angle towards the shorter nozzle lip (azimuthal angle ϕ=180°) with Mach-number increase. At the subsonic Mach numbers, the predicted deflection angles are around 9° at M_{FE}=0.6 and 10.5° at M_{FE}=1.0, which agrees fairly well with the experimental value of around 10 degrees (Ref. 13). At M_{FE}=1.56 the angle reaches nearly 19°, also consistent with experiment. Note also that the nozzle discharge coefficients for the beveled nozzle computed in the RANS stage of the simulations are in quite good agreement with the data of Viswanathan [13]: the measured discharge coefficient is ~13% less compared to the round nozzle, while in the computations the difference is 13.6% for M_{FE}=1.0 and 1.56, and 14.5% for M_{FE}=0.6. Restoring the discharge coefficient of the round nozzle would be easy with an area increase, but the deflection is more permanent. Its consequences at the aircraft system level include a thrust loss and an induced-drag increase, and are not studied here. We note however that most applications will be

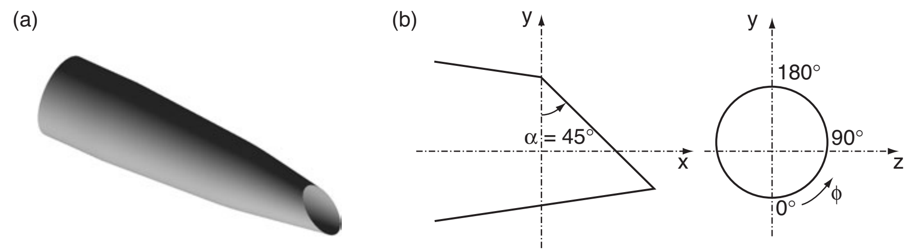

Figure 2: General view of beveled nozzle (Ref. 13) and convention on bevel (α) and azimuthal (ϕ) angles.

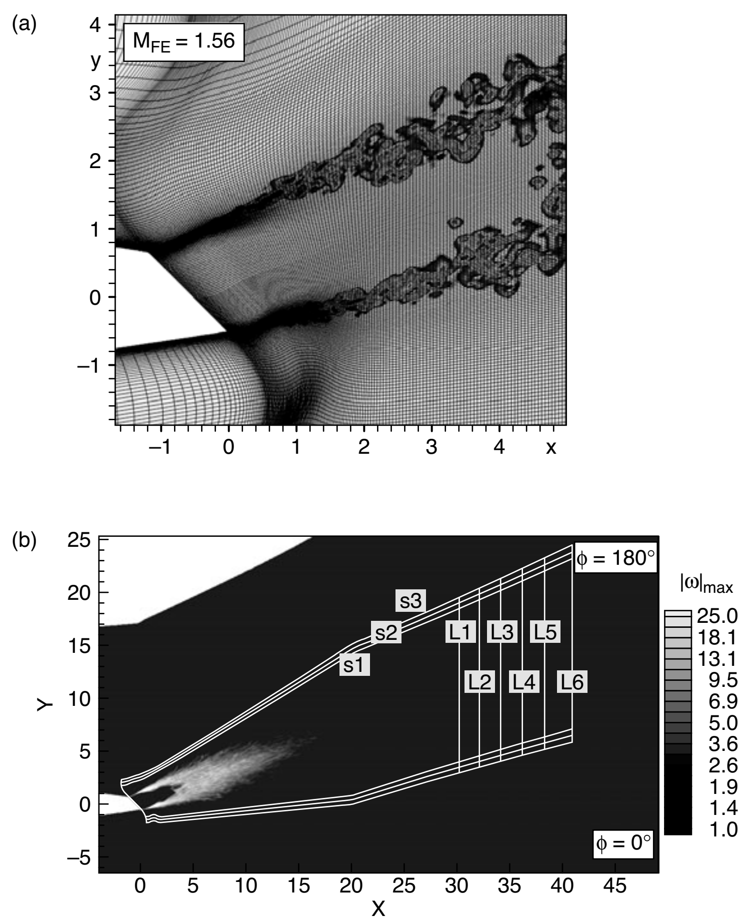

Figure 3: Fragment of LES-grid and snapshot of vorticity near exit of beveled nozzle (a), and nested FWH surfaces in *XY*-plane together with maximum (over time-sample) vorticity field (b).

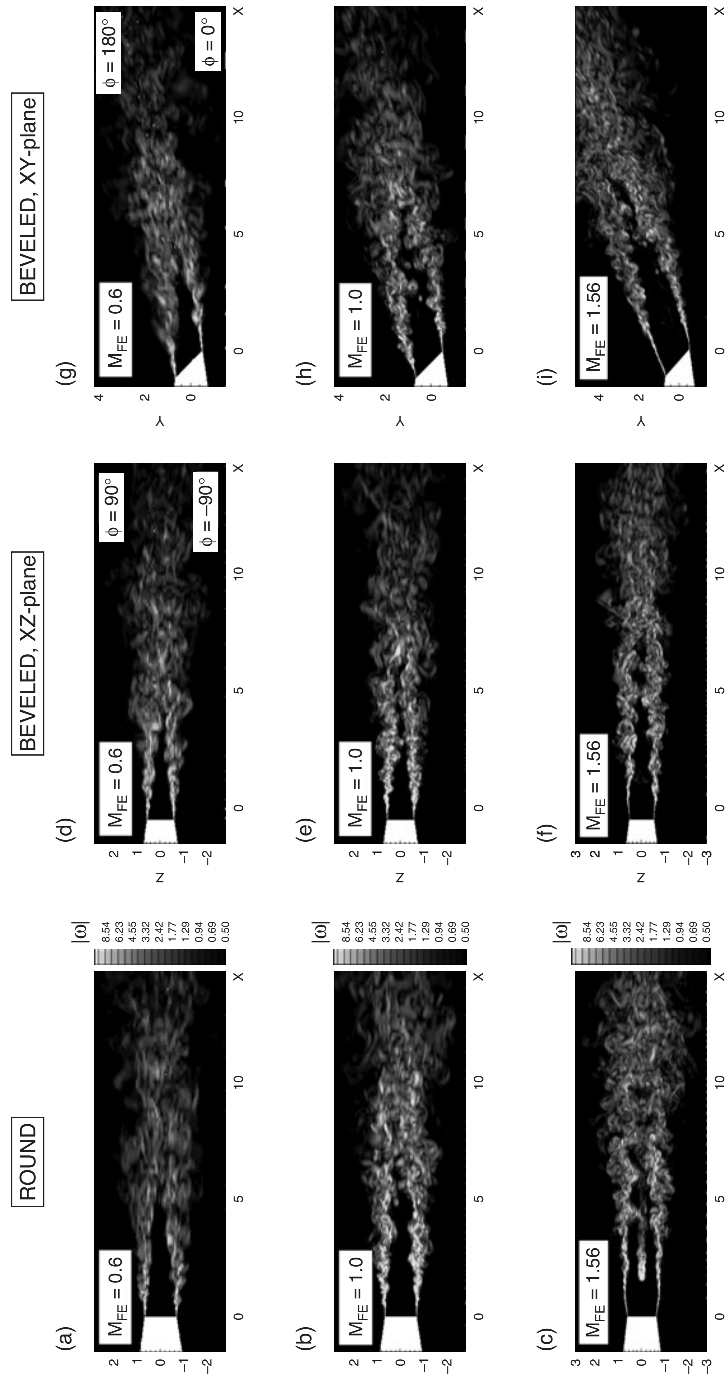

Figure 4: Snapshots of vorticity in round and beveled jets.

to turbofan engines, for which the thrust deflection could be managed in other ways. Other than that, Fig. 4 suggests that the nozzle beveling causes a narrowing of the jet in the plane normal to the symmetry plane XY and slanted to track the jet[1], while in the symmetry plane the jet is widening, the effect getting more pronounced as M_{FE} increases.

For the turbulence, a qualitative difference between round and beveled jets has so far been detected only in the supersonic flow regime. It consists in the formation of an "internal" vortical layer in the central part of the jet from the round nozzle, which is associated with the normal shock (Mach disk) and "internal" shear layer in this jet (see vorticity field in Fig.4c). In the beveled jet, the normal shock does not form.

"Numerical Schlierens" of the under-expanded round and beveled jets in the XY- and XZ -planes presented in Fig. 5 give a more detailed idea of the alteration of the wave pattern and, just as Fig.4, show that the width of the beveled jet in these two planes is rather different. This is explained by the deformation of the jet cross-section (which becomes oval) increasingly at higher bevel angle and jet velocity. The latter trend is demonstrated by Fig. 6, where the time-averaged Mach-number fields in the section x=10 D_{jet} are plotted for the jets with M_{FE} =1.56 and 0.6.[2]

One more peculiarity of the supersonic jet from the beveled nozzle, which is clearly seen from a comparison of the time-averaged magnitude of the pressure gradient in the two jets at M_{FE} =1.56 presented in Fig. 7, is a faster damping of the shocks in the beveled jet.

Not surprisingly, the above specific features of the jets from beveled nozzles result in a significant alteration of the noise generated by such jets. This is seen already in the instantaneous XY - and XZ -cuts of the pressure time derivative, in the acoustic range, for two of the considered Mach numbers in Fig. 8. This figure visually reflects the alteration of the direction of the radiated sound waves, roughly following the plume deflection caused by the beveled nozzle. As far as the effect of M_{FE} is concerned, its increase from 1.0 up to 1.56 results in stronger and shorter sound waves and, also, in a qualitative alteration of the sound-wave structure associated with the appearance of broadband shock-cell noise and Mach-wave radiation typical of high-velocity supersonic jets with strong shocks.

Finally, Fig. 9 illustrates the azimuthal non-uniformity of the sound generated by beveled jets, the effect being rather pronounced at M_{FE}=1.56 but virtually negligible at M_{FE}=0.6.

A quantitative comparison of the noise predictions with the data of Ref. 13 is presented in Fig. 10 where computed and experimental spectra (1/3-octave for the subsonic jets and narrow-band with 23.4 Hz band width for the supersonic jets) at θ = 130° are plotted for all cases. In general, the simulations reproduce the spectral shapes

---

[1] In Fig. 4 and hereafter, the projection of this plane onto the Cartesian XZ -plane is referred to as " XZ -plane".

[2] As in [2], for static jets, time averaging is started only after statistically mature turbulent fields are obtained (this typically takes 500-800 convective time units, D_{jet}/U_{jet}) and then is performed for about 200 convective time units. For jets in ambient flow, obtaining mature turbulent fields takes much less time (typically 300-400 time units). These values were picked to obtain spectra smooth enough to draw conclusions; the uncertainty drops only as fast as the inverse square root of the sample, so that extra smoothness would come at a very high cost.

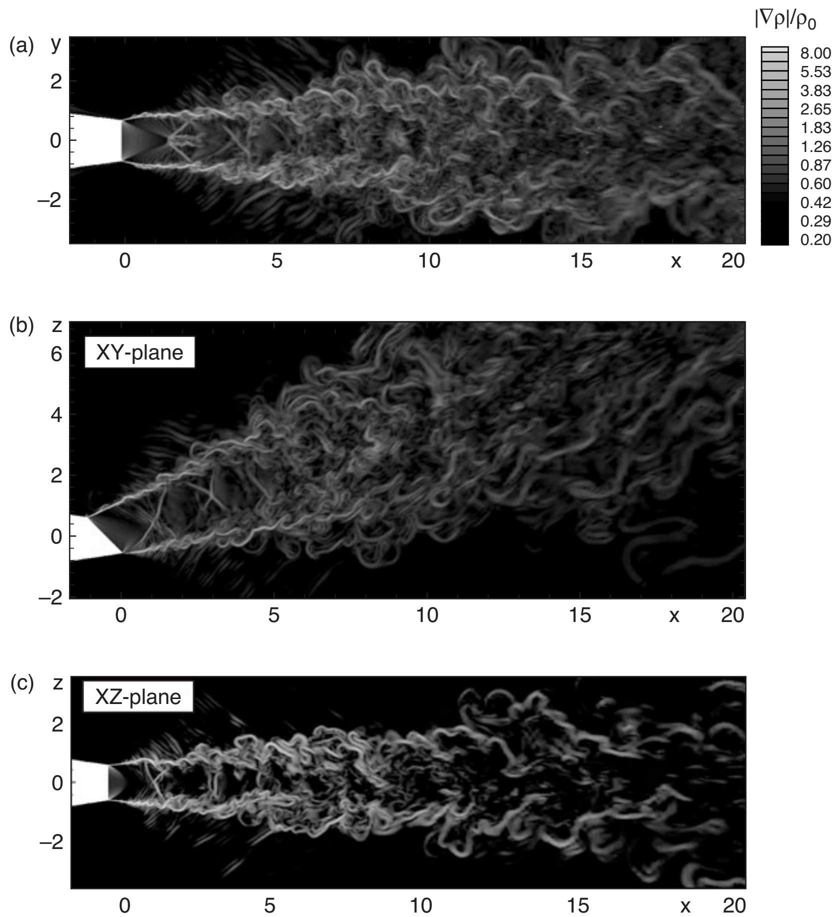

Figure 5: "Numerical Schlierens" for round (a) and beveled (b, c) nozzles at $M_{FE} = 1.56$.

fairly well and capture most of the trends observed in the experiments. The only exception is a significant underestimation of the slope of the spectral curve at the high-frequency end for the noise radiated by the supersonic beveled jet in the upward direction ($\phi = 180°$).

For the other polar angles not shown in the figure the maximum discrepancy between the predicted and experimental spectra for the round jets is within 2-3 dB everywhere, except for the directions close to the jets axis, where it reaches 4 dB near the spectral maximum. For the beveled jets, the maximum difference between the predicted and measured spectra (5-6 dB) is observed for the upward noise of the supersonic jet at the polar angles in the range $70° < \theta < 100°$, while for all the other cases the difference is close to that for the round jets.

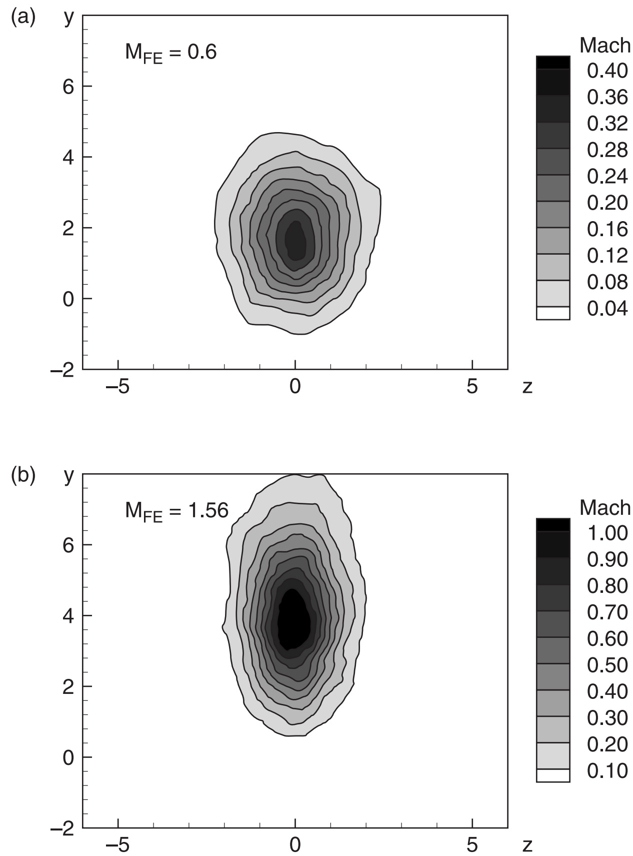

Figure 6: Mean Mach number contours in x/*D* = 10 cross-section of beveled jets at different Mach numbers.

Consistently with the described behavior of the spectra, the computed directivity curves shown in Fig. 11 also agree well with the corresponding data, except for the upward noise of the supersonic beveled jet. In particular, the figure suggests that, similar to experiment, the sideline noise of the beveled jets in the simulations is virtually the same as that of the round ones, while the downward and upward noise reduction caused by the beveled nozzle significantly depends on the Mach number (growing as M increases) and reaches ~3.5 dB for the downward noise at M_{FE} = 1.56. Note that, as mentioned above, the plume vectoring in this case is about 19°, which means a noticeable decrease of the horizontal thrust component. However, in more practical, dual, designs with beveled core nozzle this flaw is much less pronounced since the plume vectoring for such designs is not higher than 2°-4° [14].

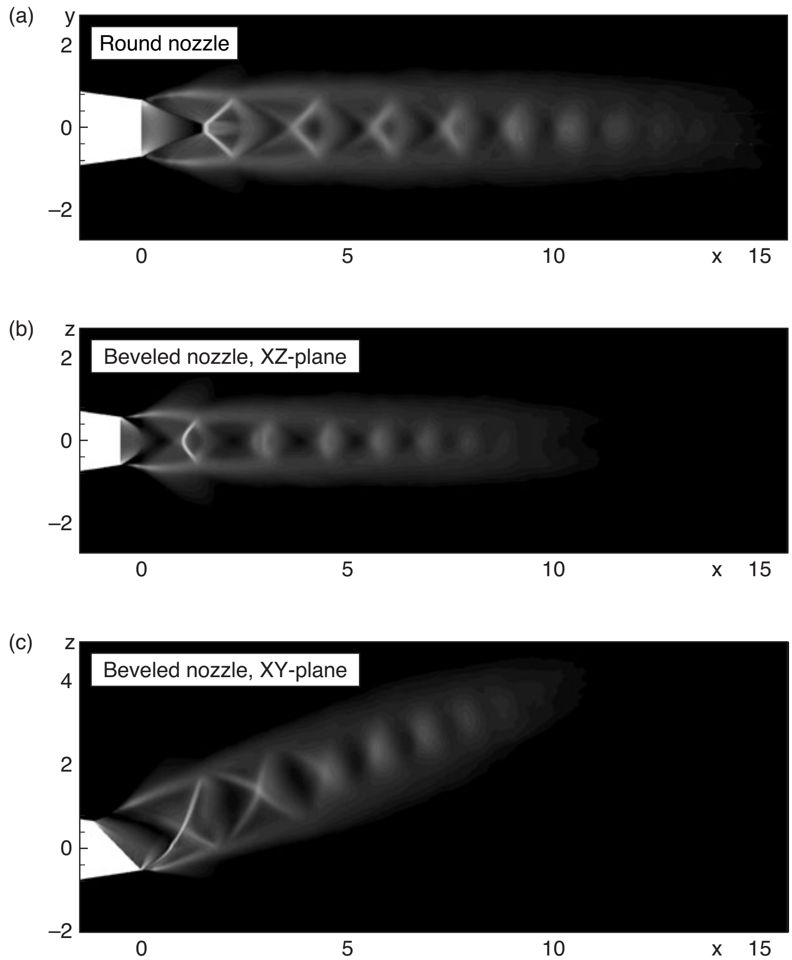

Figure 7: Time-average of magnitude of pressure gradient for round (a) and beveled (b, c) jets at $M_{FE} = 1.56$.

4. JETS FROM DUAL NOZZLES WITH FAN-FLOW DEFLECTION

The two-stream offset or deflection concept has a long history in testing, but no known practical applications. Recently a design suggested by Papamoschou [15] (see Fig. 12) was shown experimentally to provide a significant (up to 5-7 dB) peak-noise reduction in the downward direction. On the other hand, at all azimuthal angles, the noise in the direction close to the polar angle $\theta = 90°$ increased, and it seems that the success of the concept will hinge on the balance between the benefit at some angles and the penalty at others; chevrons raise similar issues. Considering this, a reliable numerical study of this noise-reduction concept could not only provide a deeper understanding, but also

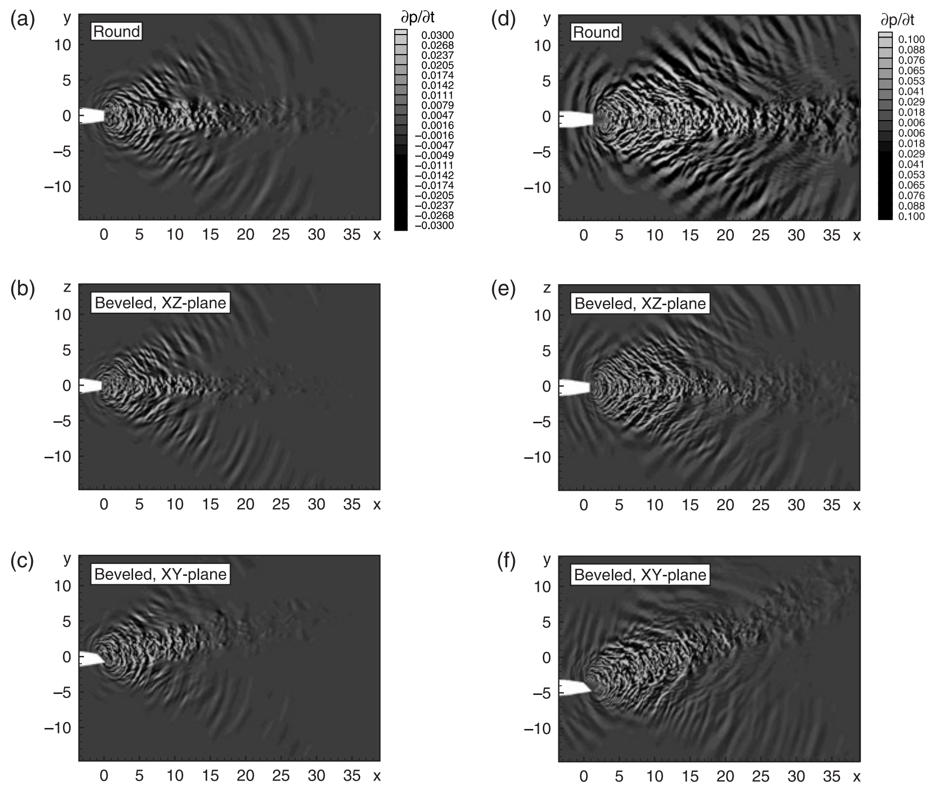

Figure 8: Snapshots of pressure time-derivative (in the acoustic range) for round and beveled jets at $M_{FE} = 1.0$ (a-c) and $M_{FE} = 1.56$ (d-f). $\partial p/\partial t$ is normalized with ρ_a, c_a, and D_{jet}.

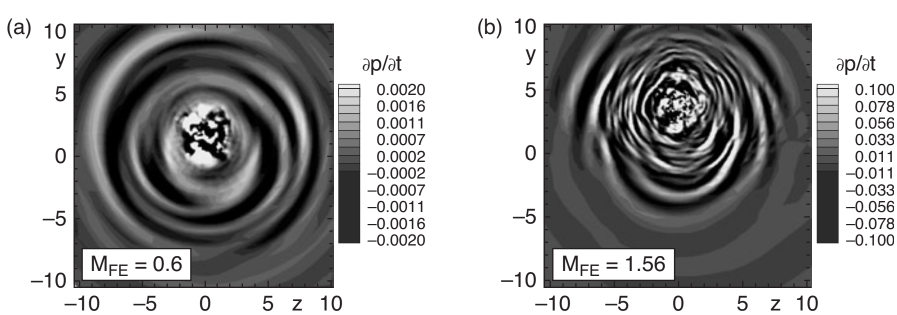

Figure 9: Snapshots of pressure time-derivative in x/D = 10 cross-section of beveled jets at two Mach numbers.

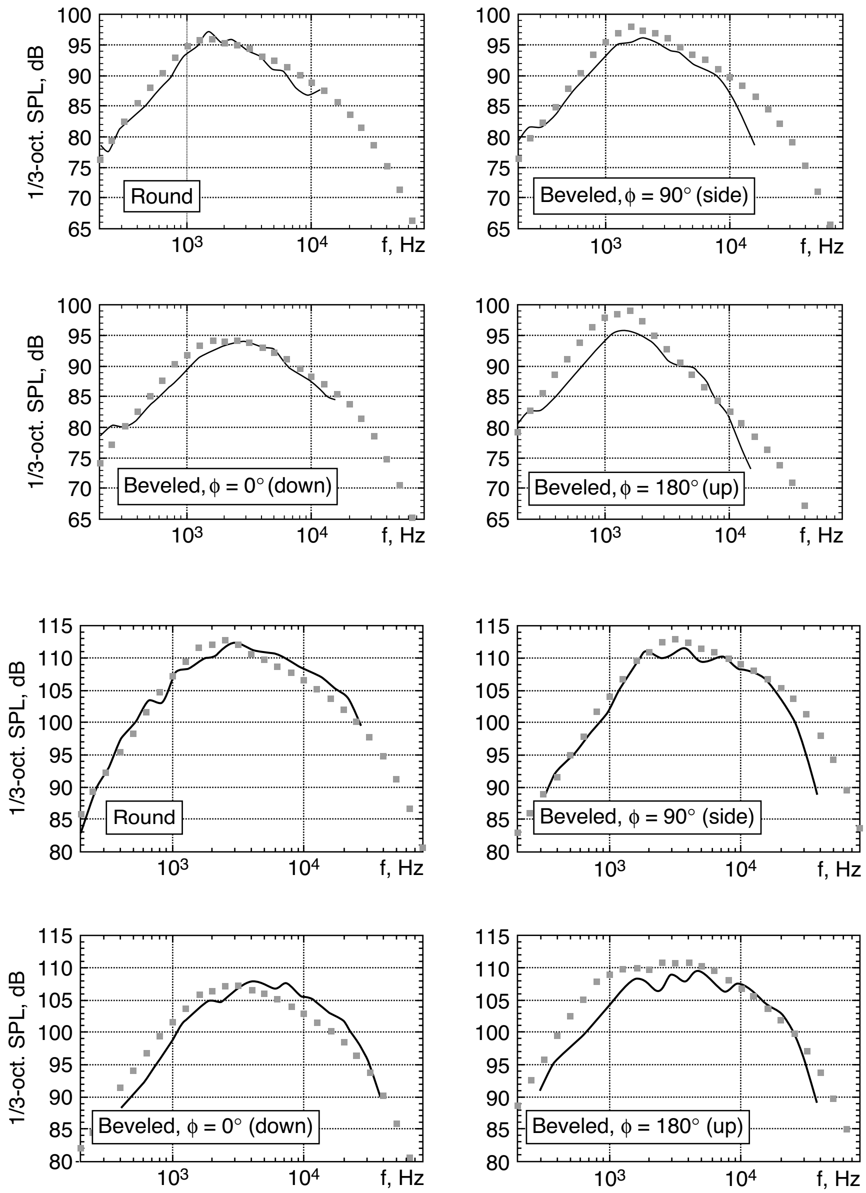

Figure 10: *(Continued)*

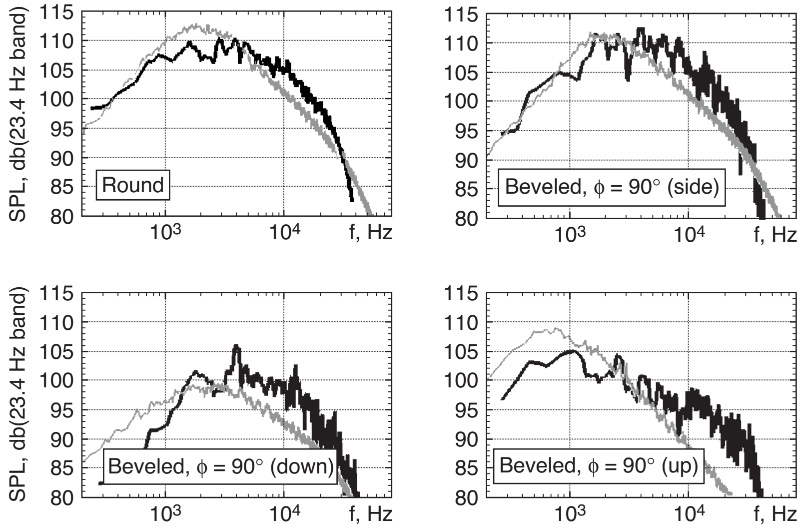

Figure 10: Computed (dark lines) and measured in Ref. 13 (symbols and light lines) 1/3-octave (frames 1-8) and narrow-band (frames 9-12) SPL spectra at $\theta = 130^{\circ}$ for round and beveled jets at $M_{FE} = 0.6$ (frames 1-4), $M_{FE} = 1.0$ (frames 5-8), and $M_{FE} = 1.56$ (frames 9-12). Distance 98 round-nozzle diameters.

suggest ways of optimising it. In addition, modern CFD analysis of the installed engines promises a much finer design capability for deflections, which are likely to remain subtle and depend on other deviations from axisymmetry, including the engine pylon and the wing.

The simulation of this flow with vanes could use the two-stage, RANS-LES, procedure presented in section 2.2.1. However, this would require gridding the full set of vanes for RANS computations, which does not seem justified at this preliminary stage, since the device used to obtain the deflection is still evolving. There are good reasons to use nozzle shaping rather than vanes, including the interaction with fan turbulence and the interference with thrust reversers. Instead, we preferred to "mimic" the effect of the vanes on the velocity field at the nozzle exit with the use of the following formulas for the components of the velocity vector $\mathbf{V}^{vanes}$ induced by the vanes (or similar devices):

$$u_{\phi}^{vanes} = -V_{\max} \frac{u_x^{base}}{U_{fan}^{base}} \frac{r_p}{r} \sin^n \phi,\ u_x^{vanes} = -2.5 V_{\max} \frac{u_x^{base}}{U_{fan}^{base}} \cos\phi \sin^n \phi, u_r^{vanes} = 0, \quad (4)$$

where u_{ϕ}^{vanes}, u_r^{vanes}, and u_x^{vanes} are the azimuthal, radial and streamwise components of $\mathbf{V}^{vanes}$;$V_{\max}$ is the parameter controlling the maximum value of the azimuthal velocity

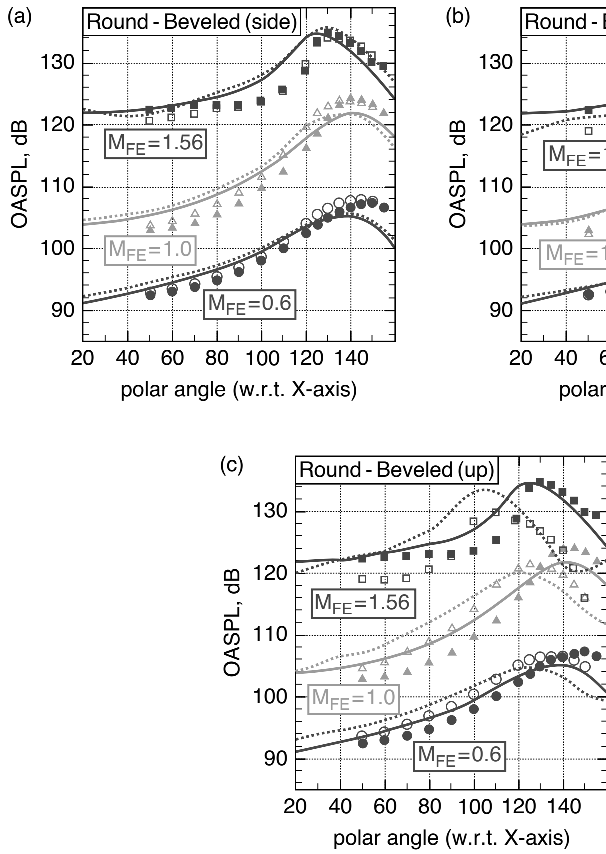

Figure 11: Computed and measured (Ref. 13) OASPL polar directivities for round (solid lines for computations, filled symbols for experiment) and beveled (dashed lines and open symbols) jets in different azimuthal directions. Distance 98 round-nozzle diameters.

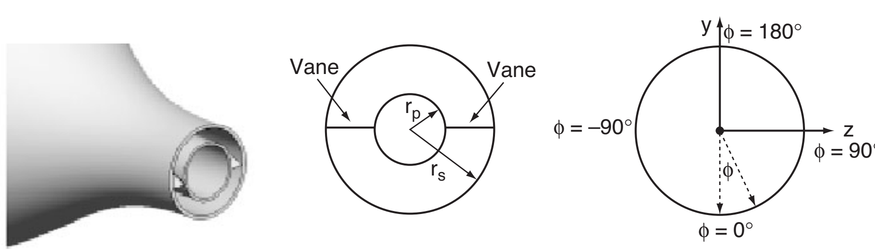

Figure 12: General view of the dual coplanar nozzles with fan-flow deflecting vanes (Ref. 15) and convention on azimuthal angle ϕ.

u_ϕ^{vanes}; u_x^{base} is the local value of the streamwise velocity component in the fan nozzle exit plane for the baseline nozzle, without vanes; U_{fan}^{base} is the value of u_x^{base} in the inviscid core of the flow; r_p is the radius of the primary (core) nozzle; and $r_p < r < r_s$ is the radial coordinate (r_s being the radius of the secondary (fan) nozzle). The parameter n is an odd integer, which controls the compactness of the velocity disturbance defined by eqns (4); it is adjusted to reflect the number of vanes, or their position upstream of the nozzle exit.

Relations (4) approximately emulate vanes installed at $\phi = \pm 90°$ or in pairs symmetric with respect to that plane, and provide an irrotational velocity field. If we assume that the streamwise velocity at the exit of the baseline fan nozzle is uniform, i.e., that; $u_x^{base} = U_{fan}^{base}$ then the plume deflection angle provided by the vanes emulated by eqn (4) can be evaluated as:

$$\tan\varepsilon = \frac{\bar{u}_y^{vanes}}{U_{fan}^{base}} = c_n \frac{V_{\max}}{U_{fan}^{base}} \frac{r_p}{r_p + r_s}, \tag{5}$$

where $\bar{u}_y^{vanes}$ is the average vertical velocity and $c_n = (2/\pi)\int_0^\pi (\sin\phi)^{n+1} d\phi.$

Accounting for the vane-induced velocities, the inflow velocity angles α_y and α_z defined by eqns (1) in section 2.2.1 can be computed as:

$$\tan(\alpha_y) = \frac{u_y^{base} + u_y^{vanes}}{u_x^{base} + u_x^{vanes}},\ \tan(\alpha_z) = \frac{u_z^{base} + u_z^{vanes}}{u_x^{base} + u_x^{vanes}}, \tag{6}$$

where u_x^{vanes}, u_y^{vanes}, u_z^{vanes} are the components of the velocity vector $\mathbf{V}^{vanes}$ computed by eqns (4).

The emulation procedure was applied to the dual co-planar jet studied in the experiments of GEAE (Ref. 34) with the following primary and secondary jet parameters: $M_p = 0.75$, $M_s = 0.85$, $T_p = 737°K$, $T_s = 311°K$, ambient flow Mach number, $M_{CF} = 0.28$; and area ratio of the nozzles, $AR = 2$. Simulations of these jets presented in Ref. 33 show a fairly good agreement with the data on both integral and spectral noise characteristics. Here these simulations were repeated with vane emulation using $n=3$ ("diffuse vane impact") and then 7 ("compact vanes impact"). The parameter $V_{\max}$ in eqn (4) was adjusted to set the "nominal" value of the deflection angle defined by eqn (5) to 4° (this value is recommended in Ref. 15 as close to optimal) at both $n=3$ and 7. The corresponding values of $V_{\max}/U_S$ are 0.267 at $n=3$ and 0.366 at $n=7$. Note that no experimental data on the effect of vanes on jets in ambient flow are available in the literature. Therefore, its numerical evaluation is very important, since the concept seems to be based on "angling" the fan shear layer away from the core flow, an effect which may strongly interact with ambient flow.

Figure 13 illustrates the effect of the vanes at the two values of n on the mean flow Mach number in the symmetry plane XY. This effect is quite visual and, based on what is known from experiments for the jet in still air (Ref. 15), is qualitatively correct. Namely, the vanes cause a shortening of the upper and an elongation of the lower

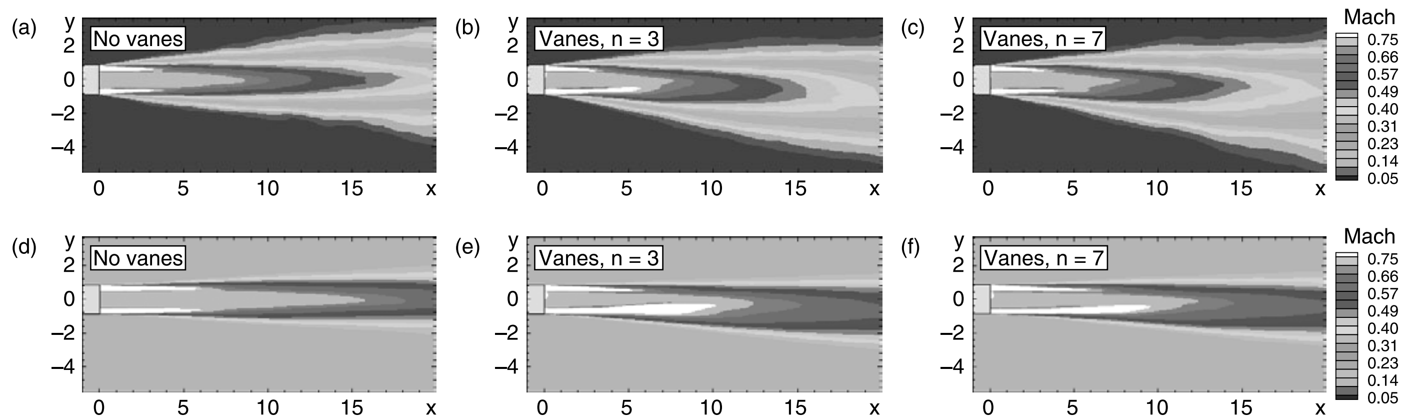

Figure 13: Effect of vanes and "vanes impact compactness" parameter n on mean Mach number fields in symmetry-plane of dual jets in still air (upper row) and in ambient flow (lower row). Lengths normalized with primary nozzle diameter.

potential cores of the fan flow, and narrowing and thickening of the corresponding shear layers. Also, the Mach number and velocity fields (not shown) reveal a "fold" in the lower shear layer as observed in experiments. For the cases with ambient flow, all these trends are the same and are even more pronounced, in spite of the lower deflection angle (about 1°, versus 3° for the entire jet in still air). As far as the influence of the compactness (the value of n) is concerned, it is nonsignificant for the quantities seen here, although at $n = 3$ the effect of vanes is somewhat stronger than at $n = 7$.

Quantitatively, the effect of the vanes on the mean flow at $n = 3$ for the jet in ambient flow is shown in Fig. 14, where we present corresponding streamwise-velocity contours in the *XY*-plane of the jet and velocity profiles in different cross-sections. In particular, the crease in the shear layer is clearly seen in the velocity profiles, which reveal a strong asymmetry of the jet. Also, the profiles in the lower shear layer have three inflexion points up to $x/D_p = 10$ at least (D_p is the diameter of the primary nozzle). In other words, the "generalized potential core" (Ref. 15) in this part of the fan flow is somewhat longer than the potential core of the primary flow (the latter is about ~$9D_p$ if defined by the ratio of centreline to inlet velocity dropping to $u_{CL} / U_p = 0.9$). The length of the generalized potential core in the upper part of the fan flow is about $5D_p$, i.e., it is shorter than the secondary potential core of the baseline flow (about $6D_p$). All these trends are also observed in the experiments and in our simulations (not shown) of the jet in still air.

Figure 15 illustrates the effect of the vanes on the cross-section of the jet in ambient flow. It shows, in particular, that the lateral deformation of the jet cross-section is somewhat stronger at $n = 7$ (compact vane impact). The deformation is caused by two pairs of streamwise vortices created by the vanes (they are seen in Fig. 15c, d, where the "in plane" streamlines are plotted together with the contours of the vorticity magnitude).

Finally, Figs. 16, 17 display the effect of the vanes on noise. Figure 16 compares the OASPL polar directivities of round jets with the corresponding jets with vanes, at different azimuthal angles. It shows that in all the cases the vanes result in a noticeable reduction of the downward OASPL in the vicinity of the peak radiation direction ($\theta =$ 140°–150°) and in some "penalty" (noise increase) for polar angles $\theta < 110°$, which comes from the high frequencies (see typical 1/3 octave spectra in Fig. 17); this is reminiscent of chevrons, and both devices inject streamwise vortices, which stretch the shear layer and therefore may directly boost the high-frequency sources. For the jet in still air the noise reduction is 4-5 dB, and the penalty is around 1 dB, while in ambient flow these numbers are 2-4 dB and ~2 dB respectively. These figures must be taken in the context of the frequency limitation of LES, as usual; it probably tends to under-estimate high-frequency penalties. Thus, the efficiency of vanes in flight seems to be somewhat lower than in still air. On the other hand, the noise reduction caused by the vanes in flight is more uniform in the azimuthal direction. Considering that sideline noise is also important for airplane certification, this cannot be ignored. The effect of the parameter n (vane impact compactness), in general, is not significant, although at $n = 3$ the azimuthal variation of the noise is somewhat stronger than at $n = 7$, which is consistent with the difference in the jet cross-section deformation discussed above.

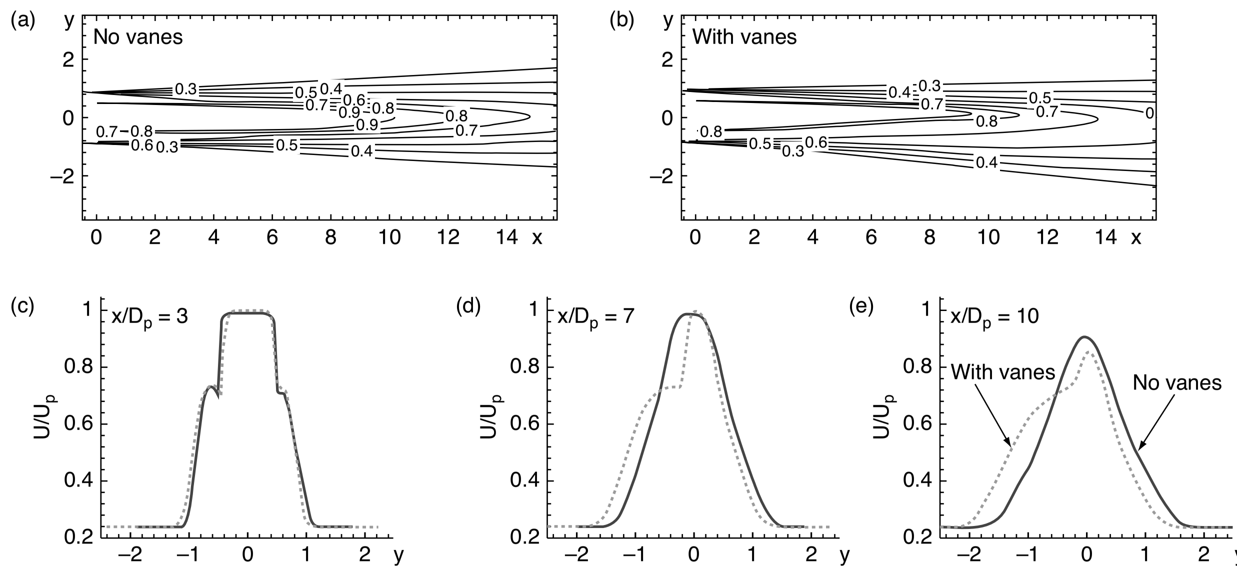

Figure 14: Effect of vanes on mean streamwise velocity contours (a, b) and profiles (c-e) in symmetry plane of dual jets in ambient flow (n = 3).

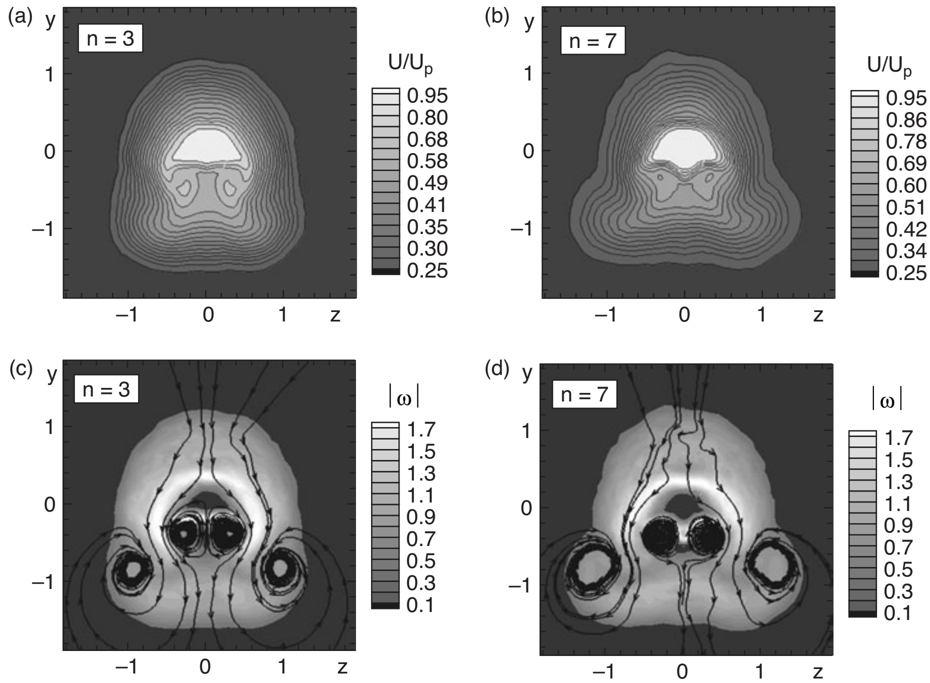

Figure 15: Effect of "vanes impact compactness" parameter *n* on mean velocity (a, b) and vorticity (c, d) fields in x/D_p=6 cross-section of dual jets with fan-flow deflection in ambient flow.

In general and with due attention to the limitations of LES, the results show that fan-flow deflecting devices are competitive with other known noise-reduction concepts, e.g., with chevron nozzles. However, it should be kept in mind that vanes may be difficult to implement in a real engine, where the fan nozzle needs to slide back to uncover the thrust reversers. This means that the vanes cannot be anchored both to the core cowl and to the fan nozzle. So from this standpoint, designs with non-axisymmetric nozzles (e.g., those with mild offsetting and/or shearing/bending of either nozzle, or with mildly beveled nozzles), which produce a jet deflection and deformation of the cross-section similar to that from vanes, may be preferable. That could be done smoothly, and may result in a similar or even a more pronounced noise-reduction effect. On the other hand, the vanes would be easier to pivot to obtain different effects at take-off and in cruise, for instance, assuming volume can be found for the mechanism.

5. JETS FROM CHEVRON NOZZLES

This noise-reduction concept is currently the most popular; the only one in airline service or in firm designs, and relatively well studied experimentally at great cost. Nonetheless, apart from the "bottom-line" effect of chevrons (decreasing the low- and

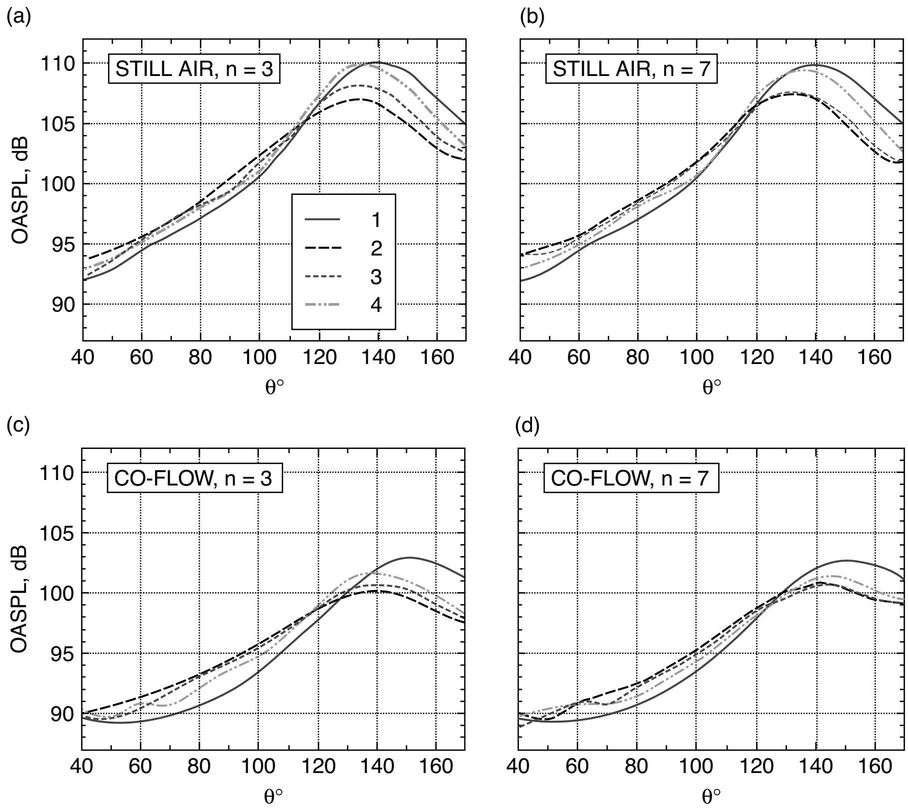

Figure 16: Effect of vanes on OASPL polar directivity of dual jets: 1 – no vanes; 2 – with vanes, $\phi = 0°$ (down); 3 – $\phi = 45°$; 4 – $\phi = 90°$ (side). Distance 166 primary-nozzle diameters.

increasing the high-frequency noise), the concept is not understood well enough to allow for an optimal design. Thus, a reliable jet noise prediction from chevron nozzle, with a full description of the turbulence field, is an important practical goal. Experimental measurements remain very slow, and of questionable accuracy in some regions for this purpose. The approach to this problem adopted here is similar to that presented in the previous section for the dual nozzles with fan-flow deflection, i.e., it is based on a chevron emulation. This is justified by the difficulty of applying in this case the full-scale two-stage procedure (see Section 2.2.1), due to the more complex shape of the exit of chevron nozzles. In addition, this would demand a much finer grid in the azimuthal direction in the LES stage in order to resolve the sharp flow-gradients in the close vicinity of chevrons' tips and valleys.

An emulation procedure based on an appropriate modification of the inflow conditions by the addition of a set of sources and sinks with zero net mass flow and in number equal to the number of chevrons, N_{chev}, was proposed in Ref. 2. In that first application, the

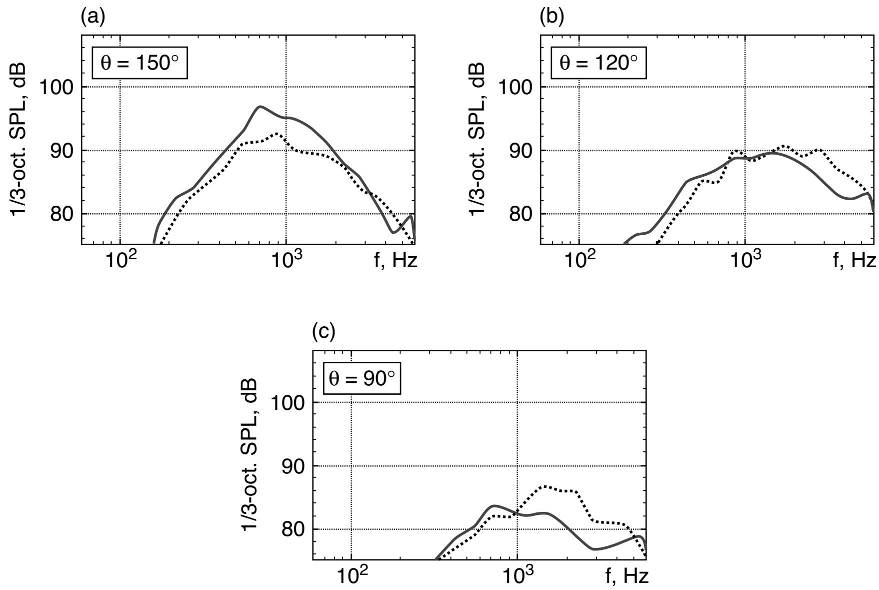

Figure 17: Effect of vanes on 1/3-octave spectra in the downward direction for dual jets in ambient flow (n = 3). Solid lines: no vanes; dashed: with vanes, $\phi = 0°$.

source/sink parameters were adjusted manually to approximately reproduce the shape of the shear layer seen in CFD solutions associated with a flight test. In the present work, this procedure is overhauled in order to link its parameters with the concrete characteristics of chevrons (their length and angle) directly, and to make it possible to account for the actual (e.g., conical) shape of the chevron nozzles in the framework of the emulation. The modified emulation procedure is as follows.

The sources and sinks (see Fig. 18) are positioned at a distance X_{SRC} upstream of the nominal exit plane of the nozzle, and at a distance R_{SRC} from the nozzle axis. The polar angles of the sources (ϕ_{kR}, ϕ_{kL}) and the sinks ($\tilde{\phi}_{kR}$, $\tilde{\phi}_{kL}$) are:

$$\phi_{kR} = \phi_k + A_\phi \frac{\Delta\phi_{chev}}{4},\ \phi_{kL} = \phi_k - A_\phi \frac{\Delta\phi_{chev}}{4},\ \phi_k = k\Delta\phi_{chev}, \tag{7a}$$

$$\tilde{\phi}_{kR} = \tilde{\phi}_k + A_\phi \frac{\Delta\phi_{chev}}{4},\ \tilde{\phi}_{kL} = \tilde{\phi}_k - A_\phi \frac{\Delta\phi_{chev}}{4},\ \tilde{\phi}_k = (k-1/2)\Delta\phi_{chev} \tag{7b}$$

where $k = 1,2,..., N_{chev}$ and $\Delta\phi_{chev} = 2\pi/N_{chev}$, and the angles ϕ_k and $\tilde{\phi}_k$ correspond to the chevron tips and valleys respectively.

Then, the velocity-vector, $\mathbf{V}^{chev}$, induced by chevrons at the point $\mathbf{r}$ of the nominal nozzle exit plane is given by

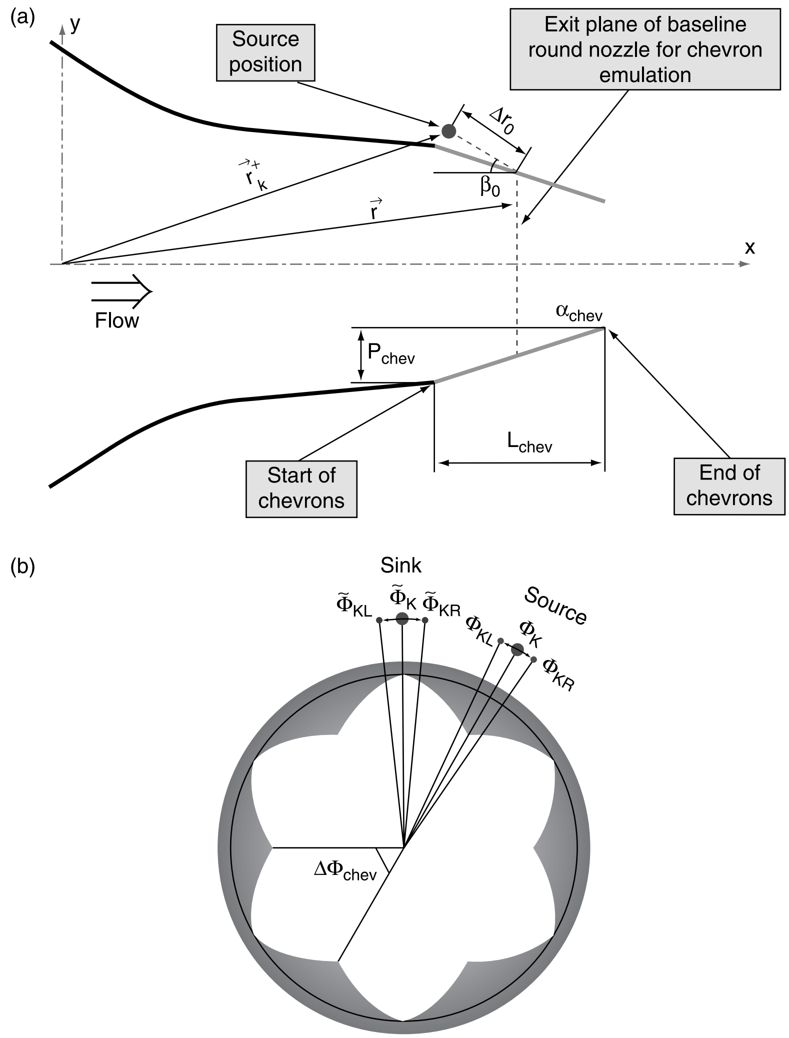

Figure 18: Schematic of chevron nozzle (a) and source/sink azimuthal position (b), with notations used in the emulation formulas.

$$\frac{\mathbf{V}^{chev}}{u_x^{base}} = \frac{1}{2} A_s P_{chev} \Delta r_0 \sum_{k=1}^{N_{chev}} \left[\frac{\mathbf{r}-\mathbf{r}_{kL}^{+}}{|\mathbf{r}-\mathbf{r}_{kL}^{+}|^3} + \frac{\mathbf{r}-\mathbf{r}_{kR}^{+}}{|\mathbf{r}-\mathbf{r}_{kR}^{+}|^3} - \frac{\mathbf{r}-\mathbf{r}_{kL}^{-}}{|\mathbf{r}-\mathbf{r}_{kL}^{-}|^3} - \frac{\mathbf{r}-\mathbf{r}_{kR}^{-}}{|\mathbf{r}-\mathbf{r}_{kR}^{-}|^3} \right], \quad (8)$$

where $P_{chev} = L_{chev} \tan(\alpha_{chev})$ is the chevron "penetration" parameter, L_{chev} is the length of chevrons, and α_{chev} is the angle between chevron and the nozzle axis. The parameter Δr_0 is the distance from the source/sink located at $\mathbf{r}_{kR}^{\pm}$, $\mathbf{r}_{kL}^{\pm}$ to the edge of the baseline round nozzle. It is made proportional to the length of chevrons:

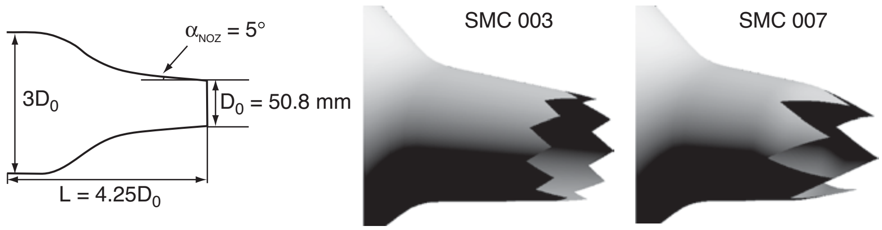

Figure 19: Geometry of round nozzle SMC000 and general view of two chevron nozzles (models SMC003 and SMC007) from Ref. 35.

$$\Delta r_0 = A_r L_{chev} \tag{9}$$

As a choice of baseline nozzle for the chevron emulation, it seems natural to identify a round nozzle, which has the same flow rate as that of the considered chevron nozzle. Based on the experiments of Bridges and Brown [35], who studied a wide variety of chevron nozzles (two of them are shown in Fig. 19), this demand is satisfied reasonably well by a nozzle with its exit plane passing through the middle of chevrons.

For the baseline nozzle just defined, a coupled (nozzle-plume) RANS computation is carried out which provides fields of total temperature and total pressure and of the background velocity vector V^{base}. The latter is used to define the inflow velocity angles (eqn (1)), which enter the inflow boundary condition for the jet-only computations with emulated chevrons, similar to what is done for the nozzle with large-scale deflection (see eqn (6)).

The emulation formulas (7)-(9) contain four "free" parameters, namely, the coefficients A_s, A_r, A_ϕ and, implicitly, the angle β_0 between the line connecting a source/sink and the nozzle edge, and the x axis (see Fig. 18). These are non-dimensional, and presumed to be universal.

Note that for a single non-split source/sink, the distribution of radial velocity at the exit of the baseline round nozzle in the meridian plane passing through the sources/sinks, u_r^{chev}, reads as:

$$\frac{u_r^{chev}(\xi)}{u_x^{base}} = \mp \frac{A_s P_{chev}}{\Delta r_0} G(\xi;\beta_0)\,, \tag{10}$$

where $\xi = l / \Delta r_0$, l is the distance to the current point from the nozzle edge, and $G(\xi;\beta_0)$ is given by:

$$G(\xi;\beta_0) = \frac{\xi + \sin\beta_0}{\left[(\xi + \sin\beta_0)^2 + \cos^2\beta_0\right]^{3/2}}\,. \tag{11}$$

A plot of the function $G(\xi)$ at different values of β_0 is shown in Fig. 20.

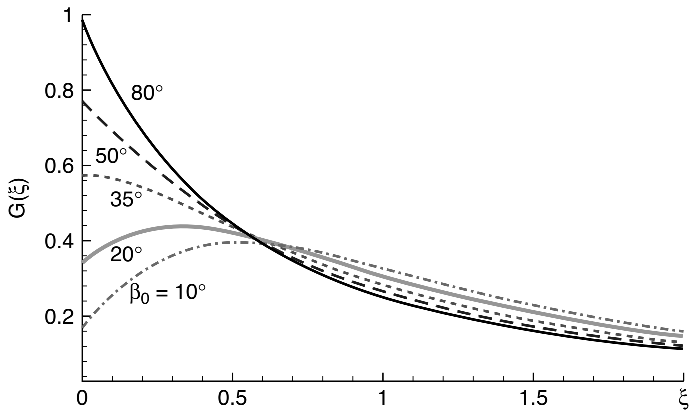

Figure 20: Effect of angle β_0 on normalized radial distribution of radial velocity induced by a single source.

Note also that with $u_x^{base} = const = U_{jet}$ the integral, $\int_0^{\infty} u_r^{chev}(l)\,dl$, characterizing the integral intensity of disturbances of velocity induced by the emulation, is equal to $\mp A_s P_{chev} U_{jet}$, i.e., it does not depend either on Δr_0 or on β_0.

This is precisely the observation which served as a guideline for choosing the form of the source in the emulation formula (8). As a result, the coefficients A_r and A_ϕ control the "compactness" of the velocity disturbances introduced by the emulated chevrons, while the coefficient A_s completely defines their integral intensity, provided that the disturbances are compact enough (A_r and A_ϕ are small). Finally, the angle β_0, as seen from the $G(\xi;\beta_0)$ plot above, controls the shape of the radial velocity distribution in the meridian plane passing through the sources/sinks, and in particular, the value of the derivative $\partial(u_r^{chev}) / \partial r$ at the nozzle wall.

The values of the emulation parameters were adjusted based on comparisons between RANS computations with gridded and with emulated chevrons for the nozzles presented in Table 1 and one of the two regimes studied in Ref. 35, namely, for a hot jet (ratio of jet temperature to the ambient $T_j / T_0 = 2.7$) with acoustic Mach number $U_j / c_0 = 0.9$ (jet Mach number 0.55). The range of angles is quite wide, and the planform of the chevrons typical of industrial applications. For this purpose, RANS solutions are sufficient, since the influence of the turbulence treatment is still very weak at the exit plane.

Note that in the course of adjustment of the emulation parameters, some observations have been made that may serve as guidelines in their choice for nozzle designs and flow regimes significantly different from those considered in the present study.

First of all, the effect of the parameter β_0 is marginal and it may always be set to 35.3° $(\sin\beta_0 = 1/\sqrt{3})$, which provides for a maximum of u_r^{chev} at the nozzle wall (see the plot

Table 1: Characteristics of chevron nozzles studied in experiments of Bridges and Brown [35]

Nozzle model	N_{chev}	a_{chev},°	L_{chev}/D_0	P_{chev}/D_0
SMC000	0	–	–	–
SMC001	6	5	0.45	0.039
SMC002	4	5	0.63	0.055
SMC003	10	5	0.28	0.024
SMC004	5	5	0.52	0.045
SMC006	6	18.2	0.45	0.141
SMC007	6	13.3	0.63	0.145
SMC008	10	13.0	0.38	0.085

$G(\xi;\beta_0)$ in Fig. 20). Second, in the rather wide range of chevrons lengths considered and at small A_r ($A_r < 0.15$), a reduction of A_r and A_ϕ results in only a weak alteration of the jet flow fields generated by the emulated chevrons, but may cause some non-smoothness of the jet boundary due to excessively compact sources/sinks. Other than that, at large A_r ($A_r > 0.2$), the emulation procedure (eqns (7)-(9)) does not permit finding a universal set of free parameters due to the interaction of the sources and sinks with each other, the "intensity" of which interaction strongly depends on the chevrons' length and number. Finally, the most important parameter of the emulation is A_s , as it directly defines the integral intensity of the disturbances introduced by the emulation, almost independently of the values of the other parameters.

Adequate values for the emulation parameters chosen based on the adjustment procedure outlined above are:

$$A_s = 0.42,\ A_r = 0.12,\ A_\phi = 0.35,\ \beta_0 = 35.3°. \tag{12}$$

In Fig. 21, as an illustration of the accuracy of representation of real chevron nozzles provided by the emulation procedure with these values of the parameters, we present contours of streamwise velocity at $x / D_0 = 1.0$, computed with the use of chevron emulation (eqns (7)-(9)), and then obtained from coupled nozzle-plume RANS solutions with the chevrons gridded, for four of the nozzles from Table 1: SMC001 and SMC007 with 6 chevrons, SMC003 and SMC008 with 10 chevrons with low (SMC001, SMC003) and high (SMC007, SMC008) penetration. The agreement is quite good.

LES and noise computations using the chevron emulation procedure outlined above were performed for two of the chevron nozzles considered in Ref. 35, namely, for SMC003 and SMC007 (see Fig. 19), and for the baseline round nozzle SMC000. The nozzles SMC003 and SMC007 represent two extremes in the design space, and in this sense they are quite representative.

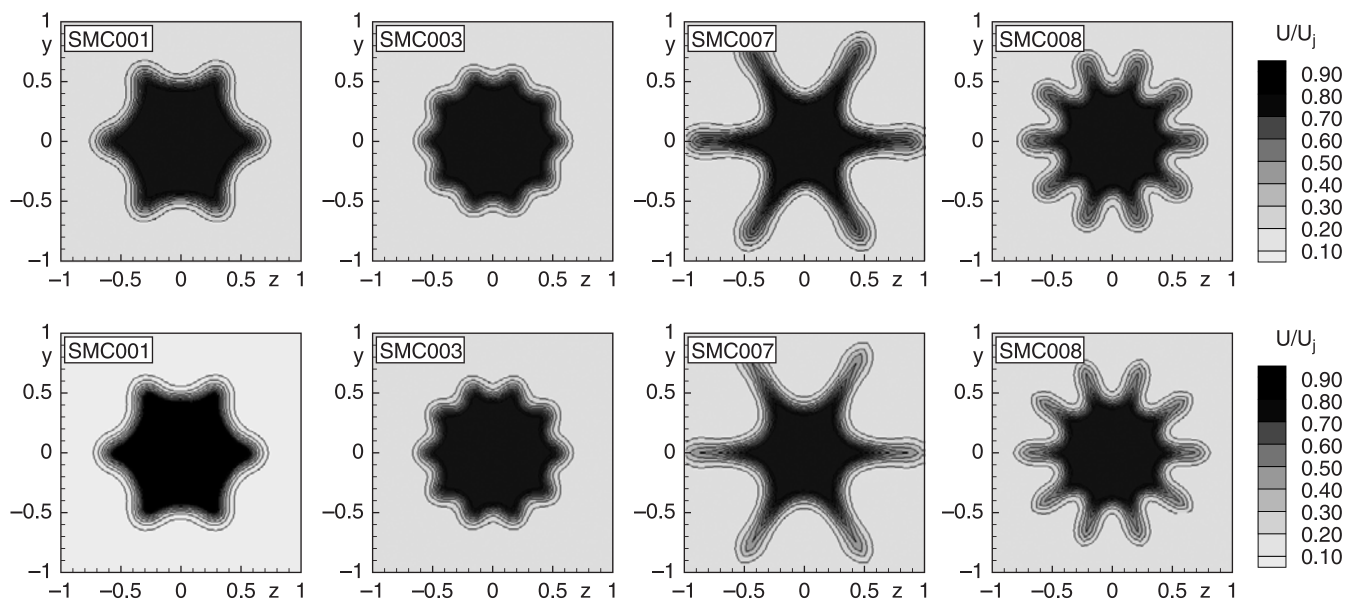

Figure 21: Streamwise velocity contours in $x/D_0 = 1$ cross-section of jets from different chevron nozzles obtained from RANS with gridding (upper row) and emulation (lower row) of chevrons. Lengths normalized with the SMC000 nozzle diameter D_0.

Indeed, according to experiments, the model SMC003 produces the weakest disturbances, and virtually does not affect the jet's aerodynamics. Nonetheless, a small reduction of the low-frequency noise near the peak radiation direction ($\theta=150°$) was observed, with no noticeable high-frequency penalty in OASPL, unlike for typical chevron nozzles. Other than that, a marginal shift of the spectrum to higher frequencies is registered at θ close to 90°, with no increase of the spectral peaks. Thus, this case permits to find out whether the emulation approach is capable of representing subtle effects seen in the experiment.

The model SMC007 is another extreme, with a strong effect of chevrons on both aerodynamics and noise. For the aerodynamics a significant decrease of the length of the jet potential core and increase of the rate of centerline velocity decay in the initial jet region were observed in the experiment. For the noise, a significant decrease at low frequencies and decrease of the spectral peaks near the peak radiation direction were observed, along with the drop of the maximum OASPL by ~3.5dB and a shift towards upstream angles (from 150° to ~135°). Other than that, the high-frequency noise at $\theta<120°$ increased significantly with a penalty in OASPL of around 1.5dB. Finally, a strong shift of the 1/3-octave spectral peaks (from St~0.5 for the round jet to St ~2-3 for SMC007) was observed at $\theta < 100°$.

An example of the grid used in LES of the chevron nozzle SMC007 together with contours of the velocity induced by chevrons in the exit plane of the nozzle is presented in Fig. 22. Note that the region with a small r -step in the grid is much thicker than in our other simulations. This is needed to provide a better resolution of the vigorously deforming jet boundary, in the absence of automatic grid adaptation. Even so, the mixing-layer transition probably is not resolved with the same detail as it is for round jets; note that this transition is strongly influenced by the stretching of the streamwise vortices. The FWH surfaces are also placed in this fine-grid region, thus providing for a better resolution of rather high sound frequencies (up to St ~4– see below).

Another specific feature of the grid is the modification in the nozzle exit plane needed to ensure a fine resolution of the initial region of the shear layers, as proposed in Ref. 2. The modification consists in decreasing the local nozzle radius at the azimuthal angles corresponding to chevron tip positions and increasing it between chevrons, with the amplitude of deformation equal to $P_{chev}/2$; this again amounts to placing the exit plane of the baseline nozzle for chevron emulation half-way between the chevron peaks and valleys. An appropriate smooth deformation of the rest of the grid in the vicinity of the nozzle exit is performed as well. The total number of nodes in the grids used is around 3 million.

Results of the simulations are presented in Figs. 23-28.

As expected, for the high-penetrating chevrons (SMC007), vorticity snapshots in the XZ -plane shown in Fig. 23 (a plane which passes between the chevrons) reveal a drastic effect of the chevrons on the flow field, in general, and on the turbulence structure in the shear layers, in particular. Transition to turbulence is very fast, the shear layers are very thick, and the potential core of the jet is much shorter than that of the SMC003 and of the round nozzle (Fig. 23a, b); this is often described as

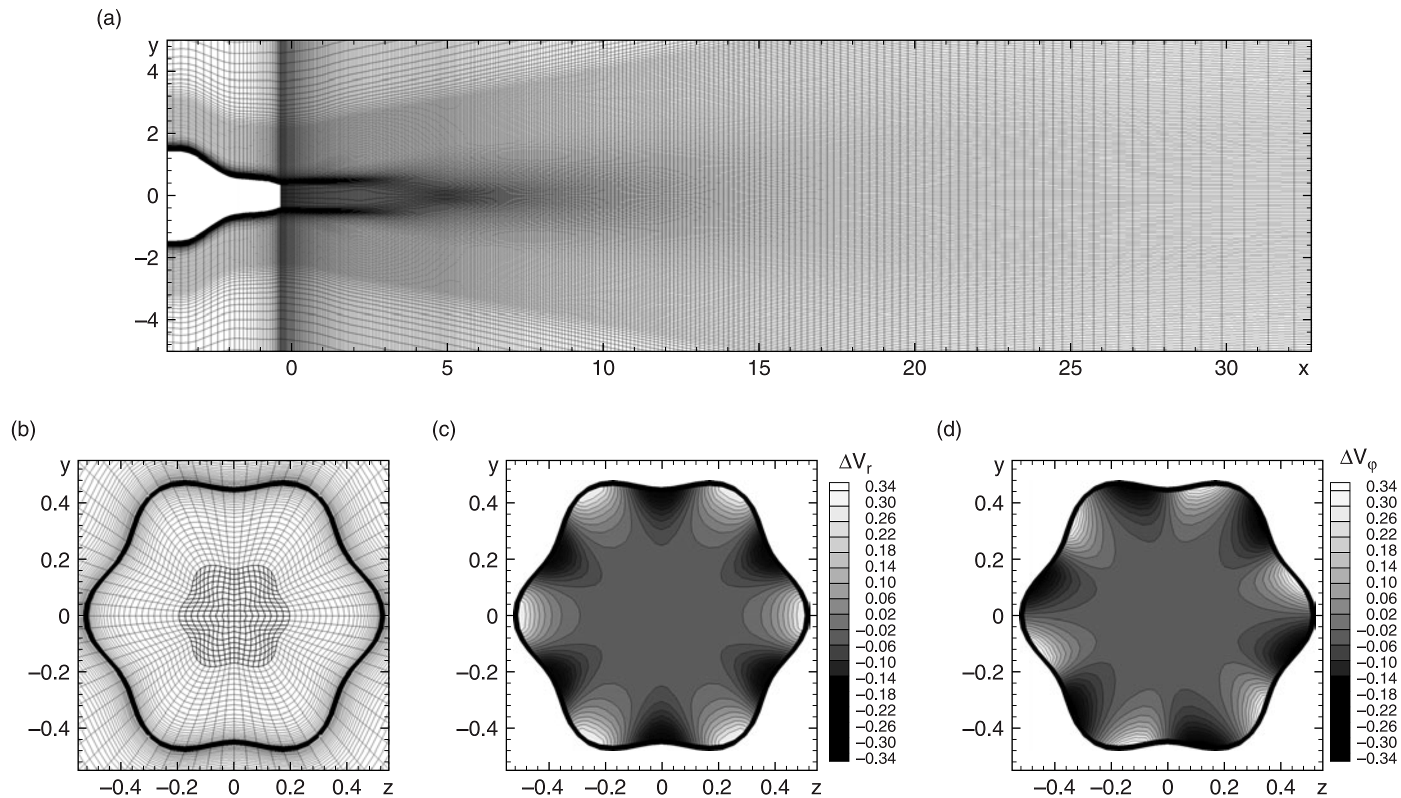

Figure 22: Fragments of grid used in LES of jet from SMC007 nozzle with chevron emulation (a, b) and "chevron-induced" velocity (eqn (8)) in nozzle exit plane (c, d).

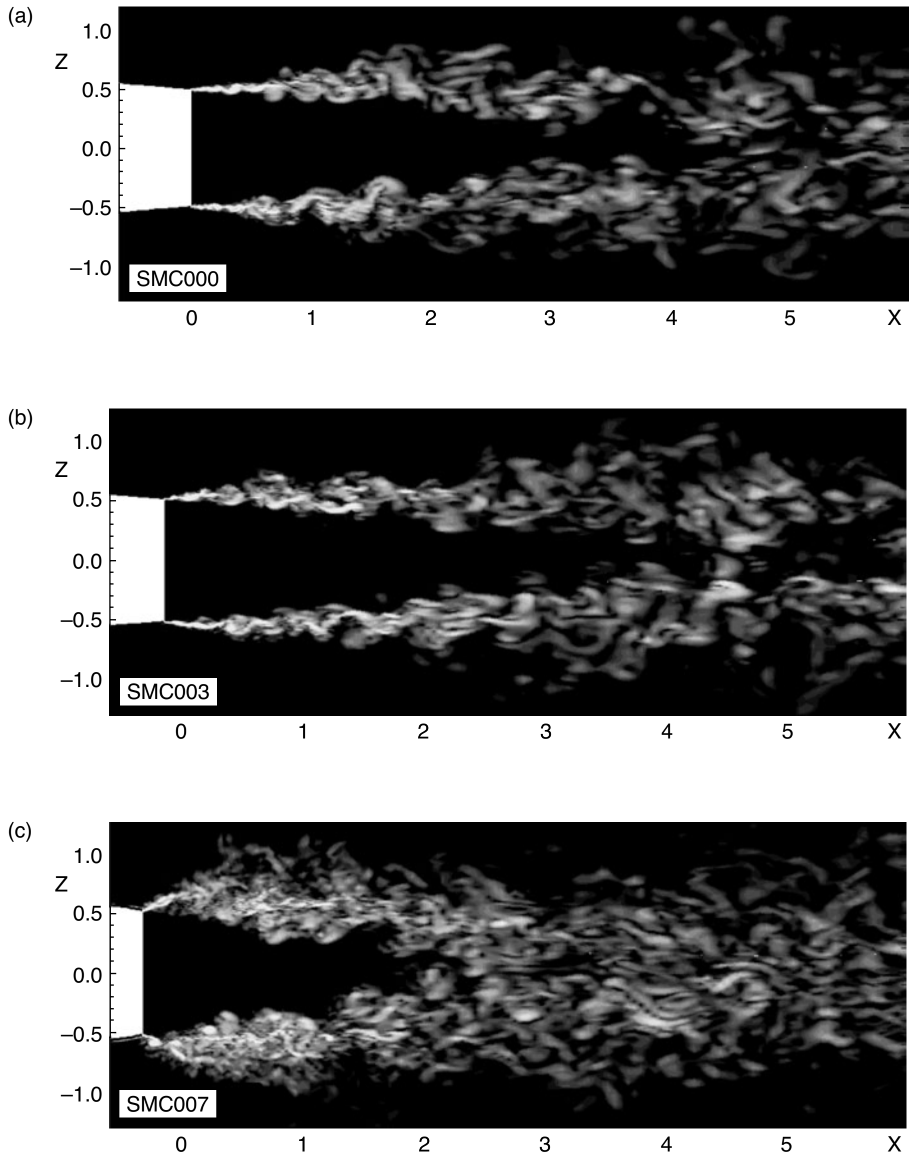

Figure 23: Snapshots of vorticity in *XZ*-plane of jets from round (a) and chevron (b, c) nozzles.

"increased mixing," unfortunately without distinction between mixing caused by stationary azimuthal variations, and mixing caused by turbulence. Other than that, a large number of small vortical structures form both in the shear layer itself and downstream of the end of the potential core of the jet, where almost no large vortices (compared with those forming in the case of the nozzles SMC000 and SMC003) are

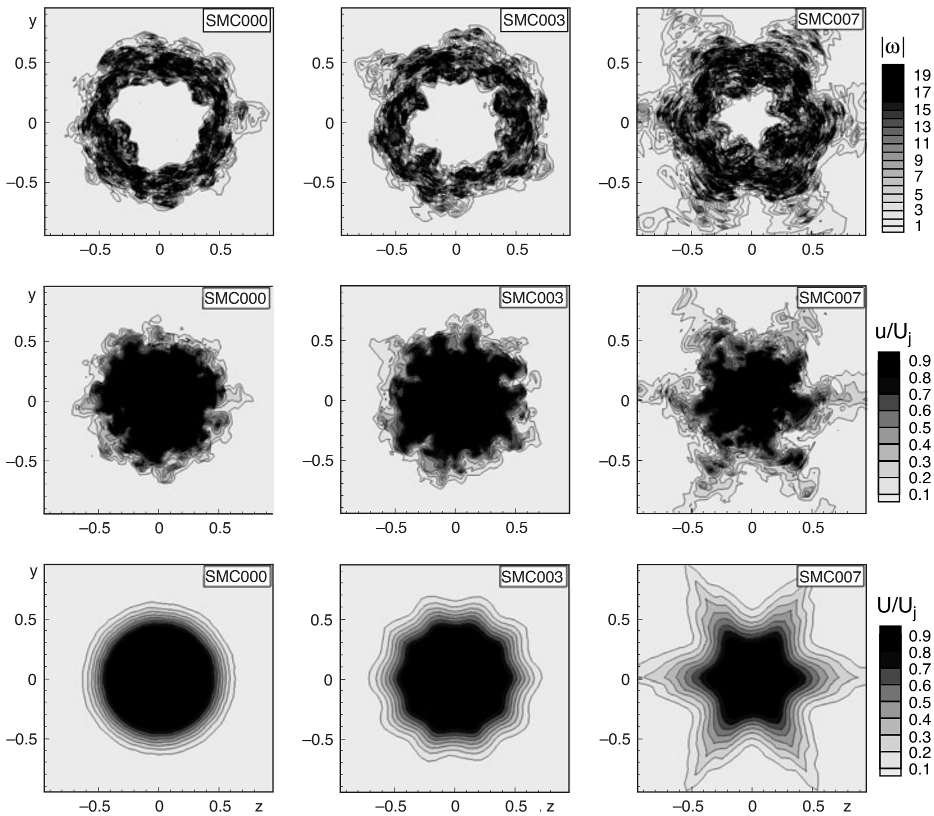

Figure 24: Snapshots of vorticity and velocity (upper and middle rows) and mean velocity contours (lower row) in $x/D_0 = 1$ cross-section of jets from round and chevron nozzles.

observed. This could be reported as a suppression of the largest eddies, and expected to reduce low-frequency noise.

Also as expected, the effect of chevrons for the nozzle with "shallow" chevron penetration (SMC003) is marginal, and the corresponding flow pattern is pretty much the same as that for the SMC000 round nozzle, except for a minor deflection of the shear layer from the jet axis in the *XZ* -plane (Fig. 23b) and in the opposite direction in the *XY* -plane (not shown).

Figure 24 presents typical *x*-cuts of the instantaneous vorticity magnitude and instantaneous and time-averaged streamwise velocity for the three jets. The vorticity snapshots reveal the same features as those discussed above with regard to the meridian cuts in Fig. 23, namely, an intensification of the fine-scale turbulent structures and a faster collapse of the jet potential core with the deeply penetrating chevrons. Other than that, in spite of the strongly chaotic instantaneous fields, the time-averaged fields are quite regular and reveal the well-known daisy-like shape of the jets; this is a testimony to the sufficient length of the time samples.

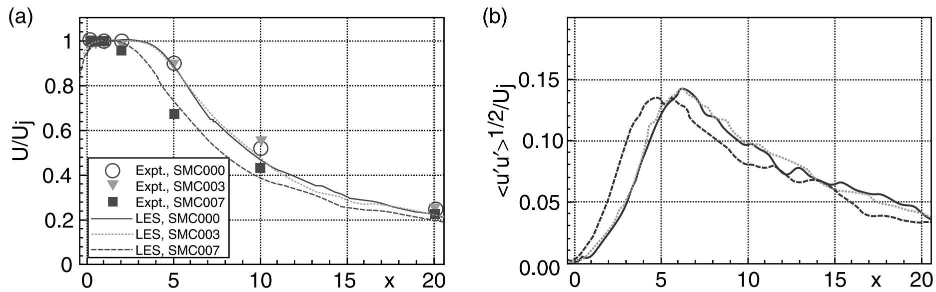

Figure 25: Computed and measured (Ref. 35) streamwise distributions of mean centerline velocity (a) and its root-mean-square fluctuations (b) for jets from round and chevron nozzles.

Unfortunately, a quantitative comparison of the flow patterns from LES of the chevron jets with the experimental surveys presented in Ref. 35 is difficult. However, qualitatively, all the trends observed in the experiments are reproduced in the simulations quite correctly. This is supported by a quantitative comparison of the predicted and measured centerline velocity distributions shown in Fig. 25. The agreement of the LES with the data is fairly good for both the length of the potential core and the rate of velocity decay for all three cases. The figure shows, also, that in the simulation, just as in the experiment, the velocity distribution for the chevron nozzle SMC003 is virtually the same as that for the round nozzle SMC000, while for the nozzle SMC007 it is quite different. The same is true for the centerline kinetic turbulence energy distributions from the simulations (these distributions are not available in Ref. 35).

Figures 26-28 present the 1/3-octave SPL spectra at four observer angles, the SPL maps, and OASPL directivities together with available experimental data. Quite consistently with the effect of the chevrons on the aerodynamic characteristics, the noise generated by the jet from the SMC003 nozzle is very close to that of the jet from the round nozzle SMC000: only a marginal reduction of the low-frequency noise in the peak radiation direction and a weak shift of the spectra to higher frequencies at $\theta = 90°$ are observed. In contrast, for the jet from the SMC007 nozzle, the reduction of both the low-frequency spectral content and OASPL in the peak radiation direction ($\theta = 130°–150°$) are very pronounced, as is the shift of the maximum of the OASPL curve to less shallow angles. At observer angles $\theta < 130°$, this jet, on the contrary, generates much louder high-frequency noise than the jets from SMC000 and SMC003 nozzles, and the corresponding spectral peaks are shifted significantly towards higher frequencies (from $St_{max} \approx 0.5–0.6$ for SMC000 and SMC003 to $St_{max} \approx 1–1.5$ for SMC007).

The agreement of the noise predictions with experiment, in general, is quite good. Somewhat unexpectedly, the best agreement is reached for the SMC007 nozzle, which has the most complex geometry and makes the shear layers most difficult to cover well. The discrepancy between the computed and measured OASPL for this case is about

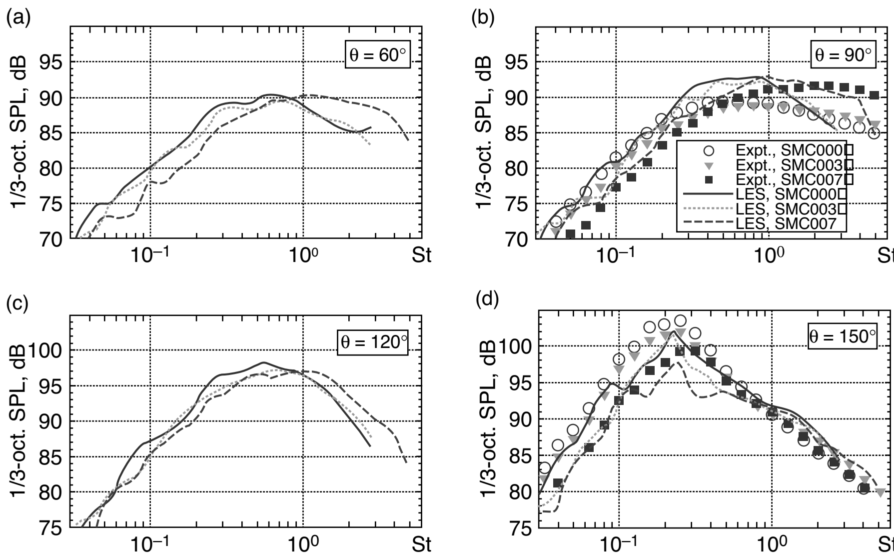

Figure 26: Computed and measured (Ref. 35) 1/3-octave SPL spectra for jets from round and chevron nozzles. Distance 40 effective nozzle diameters.

2.5 dB at $\theta = 150°–160°$, and is much less at all the other angles. The same is true for the spectra up to *St* number values as high as 4. The higher frequencies are not resolved by the grid used, which is clearly seen in the spectra (steep drop of the dash-dot curves at *St* > 4 in Fig. 26) and, also, in the SPL maps (high "density" of contours near the right boundary in Fig. 27f).

For the jets from the SMC000 and SMC003 nozzles, the agreement with experiment is somewhat worse than for SMC007. In particular, at $\theta = 160°$, the simulation underestimates the OASPL by 3.5 dB, and over the remaining angles the discrepancy is in the range of 2-3 dB. Predicted maxima of the OASPL curves are shifted versus the experimental ones by around 10° (see Fig. 28). Other than that, the spectral maxima for these two jets at $\theta = 90°$ are overestimated by around 3 dB, and the drop of the spectra after the maxima is faster than in the experiment. Considering that the grids for these jets both in the turbulent region and in the vicinity of the FWH surfaces are no coarser than the grid used for the SMC007 jet, it can be conjectured that the worse prediction of the high-frequency part of the spectra is caused not by errors in sound propagation, but by the inability of the LES to reproduce the transition process accurately enough and, in particular, to "create" small enough eddies to generate the high-frequency noise. Thus, chevrons with deep penetration help precipitate the transition to turbulence and formation of small eddies; in this sense, the simulation of jets from such chevron nozzles is easier than without or with less-penetrating chevrons.

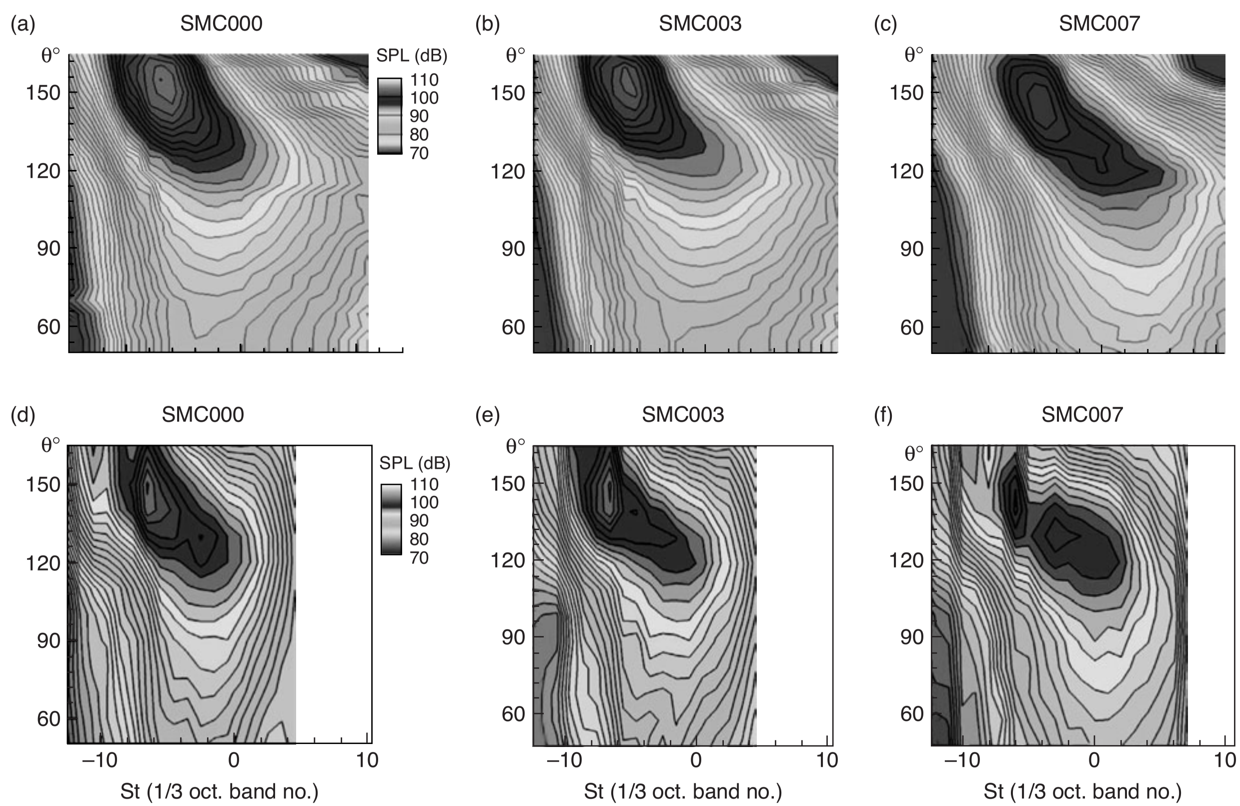

Figure 27: Measured in Ref. 35 (upper row) and computed (lower row) 1/3-octave SPL maps in the "polar angle – frequency" plane for jets from round and chevron nozzles. Distance 40 effective nozzle diameters. Band number is $10\log_{10}(St)$.

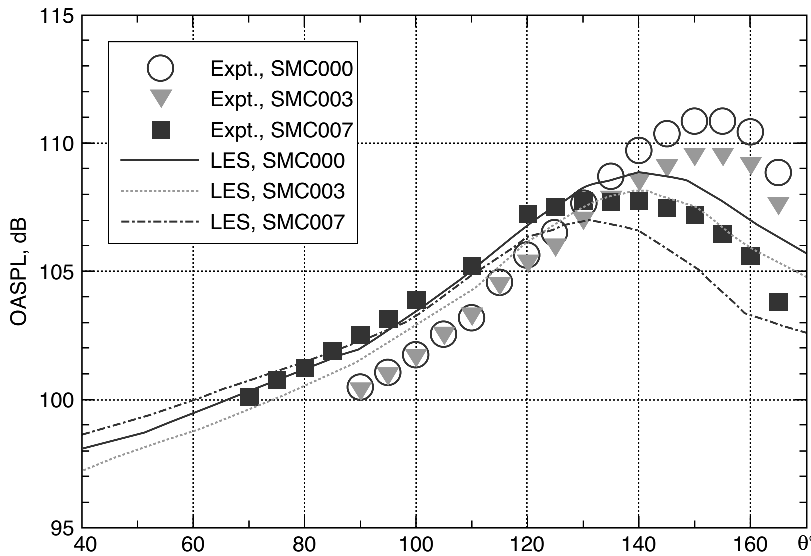

Figure 28: Computed and measured (Ref. 35) OASPL directivities for jets from round and chevron nozzles. Distance 40 effective nozzle diameters.

Finally, all three simulations predict excessively sharp spectral maxima at $\theta = 140°$–$150°$ (near $St \approx 0.22$) with some noise "deficit" on both sides of the maximum (see the spectra in Fig. 26d and SPL maps in Fig. 27d-f). It is precisely this deficit, rather than the minor underestimation of the spectral maxima themselves, which results in the underestimation of the OASPL at these observer angles.

Summarizing, based on the results presented above, it may be concluded that the simulations capture most of the experimentally observed trends in chevron effects, both on jet aerodynamics and noise. Quantitatively, the agreement with the data remains quite acceptable, even though the grid counts remain relatively small. The only two effects the simulations fail to predict are the marginal (1-1.5 dB) reduction of the spectral maximum of the noise produced by the jet from the SMC003 nozzle at $\theta = 150°$ and some (around 2 dB) increase of the spectral maximum at $\theta = 90°$ for the jet from SMC0007 nozzle. Note, also, that actually, the agreement of the simulation with the data might be even better, if we were to introduce appropriate corrections accounting for the relatively short arc-distance from the nozzles ($50D_{jet}$) at which the noise was measured in Ref. 35. The reason is that at this distance, the far-field observer angle (implied in our acoustic formulas) and the measurement angle are arguably different, because the true origin of the sound is not at the nozzle exit. Therefore, the experimental directivity curve should be shifted to lower angles if it is to predict the far-field sound field. If we consider that the source is located 2D downstream of the end of the potential core, then the shift is around 4 degrees at $\theta = 150°$ and 7 degrees at $\theta = 100°$ for SMC000 and SMC003 (the shift is less for SMC007, because breakdown is not as far downstream).

6. CONCLUSIONS AND OUTLOOK

The development of LES-based jet-noise prediction technology is proceeding, and two specific improvements are presented here, with most encouraging results. The clearest new capability is that of simulating complex non-round nozzles, but the chevron and fan-vane emulation procedures have also made significant strides, which now quantitatively link the flow fields to the nozzle geometry unlike in our earlier studies. The emphasis is on addressing the full complexity of industrial flows, both in terms of geometry and of intense flow effects such as shocks, while checking the accuracy and keeping track of the limitations of LES, especially in terms of frequency, every step of the way. At this stage, the mathematical challenges appear to have been largely mastered, and the CPU power to be the essential obstacle to unrestricted performance. An exception to this is the fact that actual aircraft geometries have additional geometry features (pylon, heat shield, vents, etc.) which will, in the long run, steer CFD towards unstructured grids; however, these have so far hardly been compatible with the high-order, low-dissipation qualities that are clearly needed of the numerics for this kind of simulation. Easy use by nonexperts will also not be achieved for quite some time. Another area for sustained attention is the mechanism of transition in the shear layers; all dependence on the grid, numerics, and (for other teams) unsteady forcing will not be eliminated for a long time. Again, CPU-power gains by orders of magnitude would remove the problem, but waiting is not an option.

The most fruitful use of LES today is to produce the turbulent fields that create the noise, thus greatly supporting the experiments which still are the core of noise-reduction technology development, because (given enough care) they cover all frequencies and their reliability is better understood than that of LES (although by no means perfect). This also has to do with the background of the current corps of noise-reduction experts. Another avenue may be the improvement of the semi-empirical models which are combined with the Acoustic Analogy and steady RANS flow fields for noise prediction at lower cost than that of LES (such methods are sometimes called "physics-based"). The experts in that field may identify the highest priorities when moving to more elaborate descriptions, in terms of anisotropy of the stress tensor or correlation patterns. LES will, at some point, suggest new inventions. For instance, a source of ideas that has not been tapped is the content of the noise in terms of azimuthal wave number m; if specific m values were found to be most damaging, devices capable of interfering with flow mechanisms at that value should be envisioned. At the simplest level, this would suggest promising values for the number of chevrons. Such information is only a matter of post-processing in LES, but would require massive instrumentation in a lab. Similarly, LES is not limited in terms of ambient flow (flight) velocity, but most experimental facilities are; another issue is that the total pressure of real fan flows is not uniform, a variation impossible to obtain from a reservoir. Further work will include a search for the cause of the remaining inaccuracies of the predictions in directions near the jet axis. Offset-stream noise-reduction concepts will be pursued, and simulations emulating the straining and offsetting effects of the wing and flaps over the jet will be considered.

ACKNOWLEDGMENTS

This work was primarily funded by Boeing Commercial Airplanes and, partially, by General Electric Aircraft Engines, under the supervision of Drs. P. Gliebe and R. Cedar and by the Russian Basic Research Foundation (grant No. 06-08-00358). The authors also thank Dr. K. Viswanathan for providing experimental data and fruitful discussions, and Prof. D. Papamoschou for his helpful comments.

REFERENCES

[1] Shur, M.L., Spalart, P.R., and Strelets, M.Kh., Noise Prediction for Increasingly Complex Jets. Part I: Methods and Tests, *International Journal of Aeroacoustics*, 2005, 4(3+4), 213–246.

[2] Shur, M.L., Spalart, P.R., and Strelets, M.Kh., Noise Prediction for Increasingly Complex Jets. Part II: Applications, *International Journal of Aeroacoustics*, 2005, 4(3+4), 247–266.

[3] Andersson, N., Eriksson, L.-E., and Davidson, L., Large-Eddy Simulation of Subsonic Turbulent Jets and Their Radiated Sound, *AIAA Journal*, 2005, 43(9), 1899–1912.

[4] Andersson, N., Eriksson, L.-E., and Davidson, L., LES Prediction of Flow and Acoustic Field of a Coaxial Jet, *AIAA Paper-2005–2884*, *11th AIAA/CEAS Aeroacoustics Conference*, *Monterey*, *CA*, 2005.

[5] Bodony, D.J., and Lele, S.K., On Using Large-Eddy Simulation for Prediction of Noise from Cold and Heated Turbulent Jets, *Physics of Fluids*, 2005, 17, 085103.

[6] Bodony, D.J., and Lele, S.K., Generation of Low Frequency Sound in Turbulent Jets, *AIAA Paper-2005-3041*, *11th AIAA/CEAS Aeroacoustics Conference*, *Monterey*, *CA*, 2005.

[7] Bogey, C. and Bailly, C., Effects of Inflow Conditions and Forcing on Subsonic Jet Flows and Noise, *AIAA Journal*, 2005, 43(5), 1000–1007.

[8] Bogey, C. and Bailly, C., Investigation of Sound Sources in Subsonic Jets Using Causality Methods on LES Data, *AIAA Paper-2005–2885*, *11th AIAA/CEAS Aeroacoustics Conference*, *Monterey*, *CA*, 2005.

[9] Lew, P., Blaisdell, G.A., and Lyrintzis, A.S., Recent Progress of Hot Jet Aeroacoustics Using 3-D Large-Eddy Simulation, *AIAA Paper-2005–3084*, *11th AIAA/CEAS Aeroacoustics Conference*, *Monterey*, *CA*, 2005.

[10] Lupoglazoff, N., Rahier, G., and Vuillot, F., Application of the CEDRE Unstructured Flow Solver to Jet Noise Computations, *Proceedings (CD-ROM) of the 1st European Conference for Aerospace Sciences (EUCASS)*, *Moscow*, *Russia*, 2005, *http://cedre.onera.fr/publications.*

[11] Paliath, U., and Morris, P.J., Prediction of Jet Noise from Circular Beveled Nozzles, *AIAA Paper-2005-3096*, *11th AIAA/CEAS Aeroacoustics Conference*, *Monterey*, *CA*, 2005.

[12] Vuillemin, A., Loheac, P., Rahier, G., Vuillot, F., and Lupoglazoff, N., Aeroacoustic Numerical Method Assessment for a Double Stream Nozzle, *AIAA Paper-2005–3043*, *11th AIAA/CEAS Aeroacoustics Conference. Monterey*, *CA*, 2005.

[13] Viswanathan, K., Nozzle Shaping for Reduction of Jet Noise from Single Jets, *AIAA Journal*, 2005, 43(5), 1008–1022.

[14] Viswanathan, K., An Elegant Concept for Reduction of Jet Noise from Turbofan Engines, *AIAA Paper-2004–2975*, *10th AIAA/CEAS Aeroacoustics Conference*, *Manchester*, *UK*, 2004.

[15] Papamoschou, D., New Method for Jet Noise Reduction in Turbofan Engines, *AIAA Journal*, 2004, 42(11), 2245–2253.

[16] Strelets, M.Kh., "Detached Eddy Simulation of Massively Separated Flows, *AIAA Paper-2001–0879*, *39th AIAA Aerospace Sciences Meeting and Exhibit*, *Reno*, *NV*, 2001.

[17] Roe, P.L., Approximate Rieman Solvers, Parameter Vectors and Difference Schemes, *Journal of Computational Physics*, 1981, 46, 357–378.

[18] Ffowcs Williams, J. E., and Hawkings, D. L., Sound Generated by Turbulence and Surfaces in Unsteady Motion, *Philosophical Transactions of the Royal Society*, 1969, A264(1151), 321–342.

[19] Dowling, A.P., Effects of Motion on Acoustic Sources, in: Grighton, D.G. et al., *Modern Methods in Analytical Acoustics: Lecture Notes*, Springer-Verlag, London, 1992, 406–426.

[20] Brentner, K. S., and Farassat, F., Analytical Comparison of the Acoustic Analogy and Kirchhoff Formulation for Moving Surfaces, *AIAA Journal*, 1998, 36(8), 1379–1386.

[21] Spalart, P.R., Shur, M.L., Strelets, M.Kh., Identification of Sound Sources in Large-Eddy Simulations of Jets, *AIAA Paper-2007-3616, 13th AIAA/CEAS Aeroacoustics Conference, Rome, Italy*, 2007.

[22] Bodony, D.J., and Lele, S.K., Review of the Current Status of Jet Noise Prediction Using Large-Eddy Simulation, *AIAA Paper-2006–0486*, *44th Aerospace Sciences Meeting and Exhibit*, *Reno*, *NV*, 2006.

[23] Lupoglazoff, N., Biancherin, A., Vuillot, F., and Rahier, G., Comprehensive 3D Unsteady Simulations of Subsonic and Supersonic Hot Jet Flow-Fields. Part 1: Aerodynamic Analysis, *AIAA Paper-2002–2599*, *8th AIAA/CEAS Aeroacoustics Conference*, *Breckenridqe*, *CO*, 2002.

[24] Shur, M.L., Spalart, P.R., and Strelets, M.Kh., Numerical Approach to the Aeroacoustics of Complex Jet Flows: Methodology, Tests, and Applications, *Proceedings (CD-ROM) of the 1st European Conference for Aerospace Sciences (EUCASS). Moscow*, *Russia*, 2005, *http://www.onera.fr/eucass.*

[25] Viswanathan, K., Shur, M.L., Spalart, P.R., and Strelets, M.Kh., Numerical Prediction of Noise from Round and Beveled Nozzles, *Turbulent Flow and Noise Generation*, *EUROMECH Colloquium 467*, *Marseille, France*, 2005, *http://www.iaq.uni-stuttqart.de/Euromech-467.*

[26] Gulyaev, A.N., Kozlov, V.E., and Secundov, A.N., A Universal One-Equation Model for Turbulent Viscosity, *Fluid Dynamics*, 1993, 28 (4), 484–494 (translated from Russian, Consultants Bureau, New York).

[27] Shur, M., Strelets, M., Zaikov, L, Gulyaev, A., Kozlov, V., and Secundov, A., Comparative Numerical Testing of One- and Two-Equation Turbulence Models for Flows with Separation and Reattachment, *AIAA Paper-1995–0863*, *33th Aerospace Sciences Meeting and Exhibit*, *Reno*, NV, 1995.

[28] Spalart, P.R., Allmaras S. R., A One-Equation Turbulence Model for Aerodynamic Flows, La *Recherche Aerospatiale*, 1994, 1, 5–21.

[29] Engquist, B., and Majda, A., Absorbing Boundary Conditions for the Numerical Simulations of Waves, *Mathematics of Computation*, 1977, 31, 629–651.

[30] Van Albada, G.D., Van Leer, B., Roberts, W.W., A Comparative Study of Computational Methods in Cosmic Gas Dynamics, *Astron. Astrophysics*, 1982, 108, 76–84.

[31] Tanna, H.K., An Experimental Study of Jet Noise. Part II: Shock Associated Noise, *Journal of Sound and Vibration*, 1977, 50, 429–444.

[32] Hill, D.J., and Pullin, D.I., Hybrid Tuned Center-Difference-WENO Method for Large Eddy Simulation in the Presence of Strong Shocks, *Journal of Computational Physics*, 2004, 194, 435–450.

[33] Shur, M.L., Spalart, P.R., Strelets, M.Kh., and Garbaruk, A.V., Further Steps in LES-Based Noise Prediction for Complex Jets, *AIAA Paper-2006-0485*, *44th Aerospace Sciences Meeting and Exhibit*, *Reno*, *NV*, 2006.

[34] Gliebe, P.R., Private communications, 2003.

[35] Bridges, J., and Brown, C.A., Parametric Testing of Chevrons on Single Flow Hot Jets, *AIAA Paper-2004-2824*, *10th AIAA/CEAS Aeroacoustics Conference*, *Manchester*, *UK,* 2004.

[36] Morfey, C.L., Wright, M.C.M., Extensions of Lighthill's Acoustic Analogy with Application to Computational Aeroacoustics, *Proceeding of the Royal Society, A*, 2007, 463, 2101-2127.

[37] Goldstein, M.E., An Exact Form of Lilley's Equation with a Velocity Quadrupole/Temperature Dipole Source Term, *Journal of Fluid Mechanics*, 2001, 443, 231–236.